

Environmental Influences on the Rapid Intensification of Hurricane Opal (1995) over the Gulf of Mexico

LANCE F. BOSART,* CHRISTOPHER S. VELDEN,⁺ W. EDWARD BRACKEN,*.@ JOHN MOLINARI,* AND PETER G. BLACK[#]

* *Department of Earth and Atmospheric Sciences, University at Albany, State University of New York, Albany, New York*

⁺ *Cooperative Institute for Meteorological Satellite Studies, University of Wisconsin—Madison, Madison, Wisconsin*

[#] *Hurricane Research Division, NOAA/AOML, Miami, Florida*

(Manuscript received 12 May 1998, in final form 25 February 1999)

ABSTRACT

Hurricane Opal intensified rapidly and unexpectedly over the Gulf of Mexico between 1800 UTC 3 October and 1000 UTC 4 October 1995. During this period the storm central pressure decreased from 963 to 916 hPa and sustained winds reached 68 m s^{-1} . Analyses that include high-resolution *GOES-8* water vapor winds and European Centre for Medium-Range Weather Forecasts (ECMWF) and National Centers for Environmental Prediction (NCEP) gridded datasets are employed to examine the rapid intensification phase of Opal.

Opal first reached tropical storm strength on 29–30 September 1995 as it interacted with a trough while situated over the Yucatan Peninsula. Opal deepened moderately ($\sim 20 \text{ hPa}$) in the 24 h ending 1200 UTC 2 October as it achieved minimal hurricane strength and as it turned northeastward. The deepening occurred in conjunction with an environmental flow interaction as determined by an Eliassen balanced vortex outflow calculation.

As Opal accelerated toward the Gulf coast by 1200 UTC 3 October, it approached the equatorward jet-entrance region of a progressive synoptic-scale trough. The trough tail extended southwestward toward the lower Texas coast. As the poleward portion of the trough moved eastward, the equatorward end of the trough lagged behind, stretched meridionally, and partially fractured as it encountered a deformation region over the northwest Gulf. Enhanced outflow and increased divergence in the upper troposphere poleward of Opal was associated with the deformation zone and the partially fractured trough tail.

An analysis of the 300–200-hPa layer-averaged divergence and 6-h divergence change based on an analysis of the water vapor winds shows a significant increase in the magnitude and equatorward extension of the divergence core toward Opal that begins at 1200 UTC 3 October and is most apparent by 1800 UTC 3 October and 0000 UTC 4 October. This divergence increase is shown to precede convective growth in the eyewall and the onset of rapid intensification and is attributed to a jet–trough–hurricane interaction in a low-shear environment. Calculations of balanced vortex outflow based on the ECMWF and NCEP gridded datasets confirms this interpretation.

A crucial finding of this work is that the jet–trough–hurricane interaction and explosive intensification of Opal begins near 0000 UTC 4 October when the storm is far from its maximum potential intensity (MPI), and the 850–200-hPa shear within 500 km of the center is weak ($2\text{--}3 \text{ m s}^{-1}$). In this first stage of rapid intensification the winds increase by almost 15 m s^{-1} to 52 m s^{-1} prior to the storm reaching an oceanic warm-core eddy. The second stage of rapid intensification occurs between 0600 and 1000 UTC 4 October when Opal is over the warm-core eddy and sustained winds increase to 68 m s^{-1} . During this second stage conditions are still favorable for a jet–trough–hurricane interaction as demonstrated by the balanced vortex outflow calculation. Opal weakens rapidly after 1200 UTC 4 October when the storm is near its MPI, the shear is increasing, and the eye is leaving the warm-core eddy. This weakening occurs as Opal moves closer to the trough. It is suggested that an important factor in determining whether a storm–trough interaction is favorable or unfavorable for intensification is how far a storm is from its MPI. The results suggest that a favorable storm–trough interaction (“good trough”) can occur when a storm is far from its MPI.

It is suggested that although the ECMWF (and to lesser extent NCEP) analyses reveal the trough–jet–hurricane interaction through the balanced vortex outflow calculation, that the failure of the same models to predict the rapid intensification of Opal can be attributed to the inability of the model to resolve the eye and internal storm structure and the associated influence of the trough–jet–hurricane interaction on the diabatically driven storm secondary circulation. The analyses also indicate that the high spatial and temporal resolution of the *GOES-8* water vapor winds reveal important mesoscale details of the trough–jet–hurricane interaction that would otherwise be hidden.

1. Introduction

The purpose of this paper is to examine the role that environmental features (trough–jet) played in the rapid intensification stage of Hurricane Opal on 3–4 October 1995. This task will be aided by taking advantage of a special dataset consisting of high-density upper-tropospheric winds derived from multispectral *GOES-8* water

@ Additional affiliation: Hurricane Research Division, NOAA/AOML, Miami, Florida.

Corresponding author address: Dr. Lance F. Bosart, 1400 Washington Ave., The University at Albany/SUNY, Albany, NY 12222.
E-mail: bosart@atmos.albany.edu

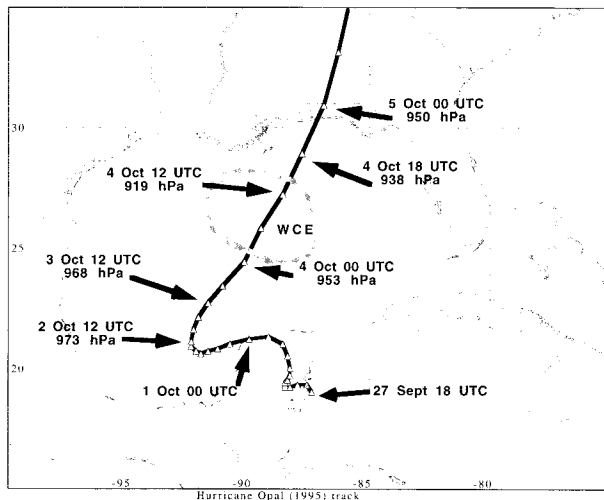


FIG. 1. Track of Hurricane Opal over the period 27 Sep–5 Oct 1995. Storm position indicated every 6 h by the open triangles. Storm central pressure (hPa) is indicated at selected time periods. Warm-core eddy (WCE) outlined in gray.

vapor (WV) imagery (Velden et al. 1997). For reference purposes the official National Hurricane Center (NHC) “best track” for Opal is shown in Fig. 1. Storm position and central pressure are indicated at selected times. The location of an oceanic warm-core eddy (WCE) traversed by Opal is also indicated in Fig. 1. A comprehensive time history of U.S. Air Force reconnaissance aircraft observations from Opal is displayed in Figs. 2a,b. Included are minimum storm surface pressure, the maximum flight-level wind speed in the primary (eyewall) and secondary (outer wind) maximum, the radius of maximum flight-level wind, and the visually estimated eye radius. Opal’s minimum central pressure and maximum wind speed were 916 hPa and 68 m s^{-1} , respectively, near 1000 UTC 4 October. Beginning near 1200 UTC 3 October, the decrease in eyewall maximum wind radius and the estimated eye radius closely parallel the decrease in storm central pressure as both numbers decrease to under 10 km near Opal’s peak intensity. A more detailed description of Opal can be found in Lawrence et al. (1998).

Our motivation for this study derives from the failure of numerical models and forecasters to predict the rapid intensification of Opal, and the desire to explore the nature of the trough–jet–hurricane interaction from an observational perspective. During the overnight and early morning hours of 3–4 October, Opal intensified explosively from a category 2 hurricane (Saffir–Simpson scale; Simpson 1974) to a strong category 4 storm. Although this unexpected overnight strengthening provided insufficient warning and evacuation time for the coastal population, a potential major disaster was averted when Opal weakened subsequent to 1000 UTC 4 October and prior to the 2000 UTC 4 October landfall (eye) over the Florida panhandle. The difficulty in fore-

casting hurricane intensity changes with Opal mirrors similar experiences with other hurricanes. Although the skill of hurricane track forecasts has improved (e.g., Burpee et al. 1996; Marks and Shay 1998), forecasting hurricane intensity change remains a challenging operational and scientific problem (Lawrence et al. 1998). Over the last 25+ yr there has been little, if any, progress at improving the accuracy of hurricane intensity forecasts (e.g., Elsberry et al. 1992; Merrill 1993; DeMaria and Kaplan 1997; Emanuel 1998; Marks and Shay 1998). The need for improved intensity forecasts is also reflected in a recent study by Neuman et al. (1997), which summarizes hurricane research needs from a forecaster’s perspective.

Hurricane intensification can be broadly related to three physical processes: 1) large-scale environmental influences, 2) storm-scale internal dynamics, and 3) ocean–atmosphere interactions. These processes may act individually or collectively, and all three may be important at different times in a storm’s life cycle. Interactions between hurricanes and external larger-scale circulations have been shown to be important to hurricane intensity changes in many papers over the last 50 yr (e.g., Riehl 1948, 1950; Palmer 1951; Simpson 1952; Koteswaram and George 1957; Ramage 1959; Yanai 1961; Colón and Nightingale 1963; Erickson 1967; Sadler 1976; Frank 1977; Pfeffer and Challa 1981; Velden 1987; Merrill 1988a,b; Lee et al. 1989; Molinari and Vollaro 1989, 1990; Challa and Pfeffer 1990; Bosart and Bartlo 1991; Montgomery and Farrell 1993; Wu and Emanuel 1993; Molinari et al. 1995; Bosart and Lackmann 1995; DeMaria 1996; Elsberry and Jeffries 1996; Merrill and Velden 1996; Briegel and Frank 1997; Shi et al. 1997; Challa et al. 1998; DeMaria and Huber 1998; Krishnamurti et al. 1998; Molinari 1998; Molinari et al. 1998; Zehr 1998). As noted by Molinari (1998), important unresolved issues regarding hurricane–trough interactions include 1) what is meant by a trough interaction, 2) how does a synoptic-scale trough interact with a mesoscale hurricane, 3) what is the role of vertical shear, 4) how do the core dynamics respond to the interaction, 5) how does the nature of the interaction vary as a function of the storm maximum potential intensity, and 6) how do identifiable parameters exist to predict whether the interaction will lead to storm strengthening or weakening? In this paper we will address these issues.

Theoretical studies of hurricane intensity changes have concentrated on storm internal dynamical processes, storm–environmental flow interactions, and storm–ocean interactions. Internal dynamical processes associated with eyewall convection have been the focus of several studies of hurricane intensity change. One unresolved theoretical issue is how axisymmetric and asymmetric processes in the hurricane contribute to intensity changes. Both axisymmetric and asymmetric convective structures are observed in hurricane eyewalls. Shapiro and Willoughby (1982) showed that con-

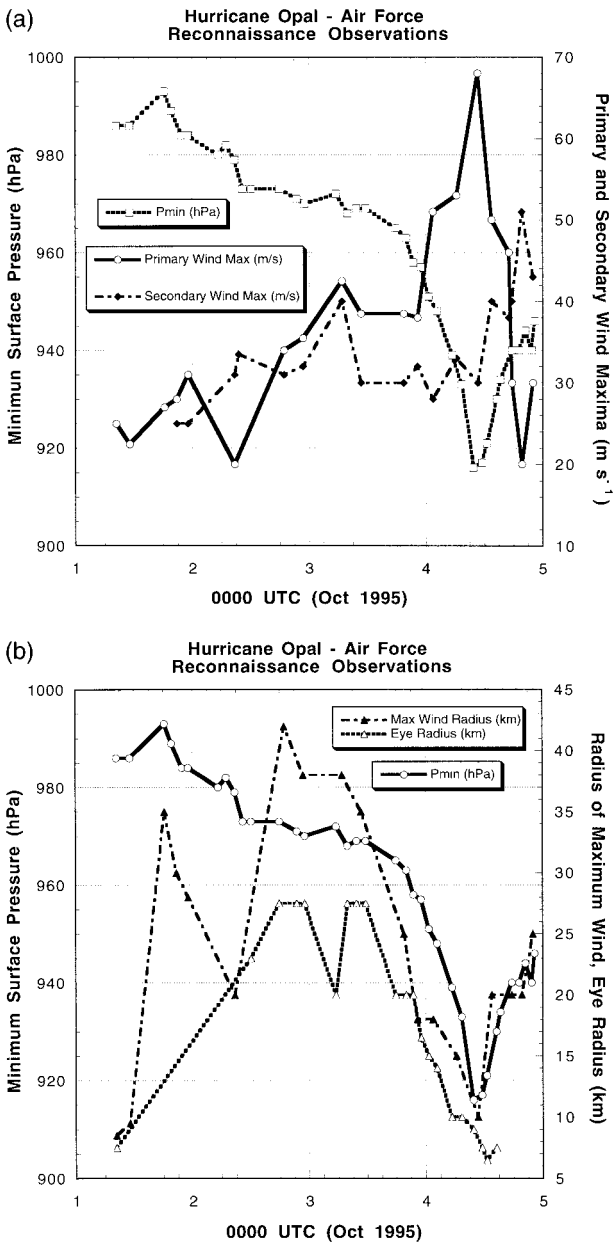


FIG. 2. Time history of selected variables as measured by U.S. Air Force reconnaissance aircraft for the period 0000 UTC 1–5 Oct 1995 (tick marks along top and bottom every 3 h). (a) Storm central pressure (dashed line with open squares, hPa), primary and secondary wind maximum (thick solid line with open circles and dash-dot line with solid diamonds, respectively, m s^{-1}). (b) Storm central pressure (solid line with open circles, hPa) with the radius of maximum wind (dash-dot line with solid triangles, m s^{-1}) and eye radius (dotted line with open triangles, km).

centric eyewall cycles could be associated with storm intensity fluctuations, a process that was mostly axisymmetric. Willoughby and Black (1996) demonstrated in the case of Hurricane Andrew (1992) that asymmetric fluctuations in eyewall convection could be associated with detectable variations in eyewall wind speeds as

Andrew approached the Florida coast. Montgomery and Kallenbach (1997), Montgomery and Enagonio (1998), and Montgomery (1998) have shown theoretically that asymmetric convection can produce intensification by axisymmetrizing localized potential vorticity (PV) maxima and that vortex Rossby waves play an important role in this process.

Atmosphere–ocean interactions also appear to play an important role in hurricane intensity change (e.g., Emanuel 1986; Rotunno and Emanuel 1987; Emanuel 1991; Khain and Ginis 1991; Shay et al. 1992; Bender et al. 1993; Holland 1997; Black and Shay 1998; Holland and Wang 1998; Hong et al. 2000; Shay et al. 2000). In the case of Opal, Black and Shay (1998), Hong et al. (2000), and Shay et al. (2000) showed that rapid intensification began as the storm neared and crossed over a WCE that was situated to the west of the warm loop current (LC). Shay et al. (2000) and Black and Shay (1998) also showed that prior to the development of Opal, the sea surface temperatures (SSTs) over the Gulf of Mexico were a quasi-uniform 28° – 29°C and that the WCE was only faintly distinguishable from the surrounding water on the basis of the SSTs alone. The WCE, represented by a mesoscale pocket (~ 250 – 300 -km diameter) of subsurface anomalously warm water (or, equivalently, anomalously high oceanic heat content), was traversed by Opal as the storm rapidly intensified. Black and Shay (1998) showed that because of the deep mixed layers in the WCE, and the rapid forward motion of the storm, no mixed-layer cooling of the WCE occurred due to ocean response processes as Opal traversed the WCE. Shay et al. (2000) showed that the WCE could be detected as an upward bulge in sea level (~ 50 cm) by the space-based altimeter flown aboard the National Aeronautics and Space Administration's oceanographic Topography Experiment (TOPEX) mission satellite (sea level heights were elevated in the WCE because of the anomalously high oceanic heat content through the top ~ 100 m of water). A modeling study by Hong et al. (2000) suggested that roughly 25% (~ 10 – 15 hPa) of the observed pressure fall during the rapid deepening phase of Opal could be explained by WCE-induced oceanic heat fluxes.

This paper will focus on the interaction between an upper-tropospheric trough–jet system and Hurricane Opal and the possible role of these interactions in the rapid intensification of the storm. This task will be accomplished through diagnostic analyses of a special high-density wind dataset derived from *GOES-8* WV imagery and gridded datasets provided by the European Centre for Medium-Range Weather Forecasts (ECMWF) and the National Centers for Environmental Prediction (NCEP). Section 2 will present a brief overview of Opal's life cycle. Our analysis methodology is described in section 3. The results from a detailed analysis of the high-density WV wind dataset and the ECMWF–NCEP gridded datasets and special remotely sensed datasets

will appear in section 4. The conclusions will follow in section 5.

2. Opal synopsis

As shown by Bracken and Bosart (1998), a disturbance in the lower-tropospheric easterlies could be seen tracking slowly westward across the Caribbean as early as 21 September. This low-level disturbance strengthened (as judged by an increase in the areal extent of convective cloudiness viewed from satellite imagery; not shown) on 22–23 September as it interacted with a southwestward-moving potential vorticity (PV) anomaly in the upper troposphere. The PV anomaly originated along a meridionally oriented 200-hPa shear line over the western Atlantic Ocean. Over its life cycle this PV anomaly could be tracked from east of Florida, across Cuba and the northwestern Caribbean, across Central America, and into the eastern tropical Pacific (Bracken and Bosart 1998). Subsequent to its interaction with this migratory PV anomaly, the pregenesis Opal disturbance continued moving westward with little intensity change through 1200 UTC 26 September. Over the next 24 h the pregenesis Opal disturbance strengthened somewhat without any apparent interaction with a PV anomaly aloft. Late on 27 September the NHC designated the disturbance, now situated just to the east of the Yucatan Peninsula, a tropical depression (Fig. 1).

The tropical depression strengthened before moving onshore over the Yucatan Peninsula at 0000 UTC 28 September. Over land it weakened slightly for the first 12 h (until 1200 UTC 28 September) and then reintensified to tropical storm strength on 29–30 September while still over land (Bracken and Bosart 1998). Opal's interaction with a second upper-tropospheric PV anomaly that fractured from the equatorward end of a mid-latitude trough over the southern United States and moved southeastward across the Gulf of Mexico and the Yucatan Peninsula provided a favorable environment for the storm's intensification (shown in Bracken and Bosart 1998).

To help bolster this argument, layer-averaged (350–355 K) PV, winds, and pressure are mapped in Fig. 3 at 12-h intervals for the period 0000 UTC 28 September–1200 UTC 3 October. The calculations are made using the Gempak software package (Koch et al. 1983) and are based upon the NCEP $2.5^\circ \times 2.5^\circ$ gridded analyses from the Global Data Assimilation System (GDAS). In the 36 h ending 1200 UTC 29 September a PV anomaly (#2 in Bracken and Bosart 1998) fractures from the main PV reservoir over the United States and moves southeastward toward the Yucatan Peninsula (Figs. 3a–d). As an area of positive PV advection ahead of the fractured PV anomaly overspreads the Yucatan Peninsula on 29 September (Figs. 3c,d), Opal intensifies to tropical storm strength (by 0000 UTC 1 October Opal deepens to 994 hPa with winds in excess of 20 m s^{-1}). This upper-tropospheric PV anomaly then stalls and re-

mains near Opal through 1200 UTC 2 October (Figs. 3e–j). Within the limitations of the coarse-resolution NCEP GDAS analyses, a close inspection of Figs. 3f–i indicates that weak positive PV advection (confirmed by direct calculation, not shown) prevails just to the west of Opal (Bay of Campeche) as the storm moves slowly westward through 0000 UTC 2 October and deepens 9 hPa to 984 hPa over the previous 12 h.

Beginning near 0000 UTC 2 October Opal turns poleward, accelerates slowly, and achieves minimal hurricane status. Opal's central pressure decreases an additional 11 hPa to 973 hPa by 1200 UTC 2 October as sustained winds reach 35 m s^{-1} . By 1200 UTC 3 October Opal deepens further to 968 hPa, sustained winds increase to near 40 m s^{-1} , and the weak PV anomaly near Opal reintensifies (Figs. 3k,l). Potential vorticity anomaly reintensification (potentially an artifact of the NCEP GDAS analysis) occurs as Opal approaches the equatorward end of a larger-scale trough (and associated jet) situated over the central United States. The coarse-resolution NCEP GDAS analysis precludes us from saying whether the apparent PV anomaly reintensification near Opal is a manifestation of the deepening of the cyclonic core of the storm or an external trough interaction. Potential vorticity also increases over southern Texas as the equatorward end of the central United States trough moves east and slows (Figs. 3k,l). Outflow from Opal reinforces the confluent flow in the jet-entrance region poleward of Opal (Fig. 3l).

A long jet "tail" extends west-southwestward across Texas and northern Mexico by 1200 UTC 3 October (Fig. 3l). A smaller-scale trough, manifest by an area of positive PV advection (estimated from Fig. 3l), appears to be embedded in this jet tail over southern Texas. A more significant area of positive PV advection is now evident poleward of Opal at 1200 UTC 3 October (Fig. 3l). Positive PV advection increases here in response to 1) the development of an area of low PV over northwestern Florida and along the central Gulf coast as the outflow from Opal strengthens and becomes more anticyclonic, and 2) the strengthening of the upper-tropospheric PV anomaly near Opal. The development of the low PV region in the Opal outflow plume is likely a reflection of diabatic processes associated with widespread latent heat release as has been shown observationally in hurricanes (e.g., Molinari 1993; Merrill and Velden 1996), extratropical cyclones (e.g., Dickinson et al. 1997), and theoretically (e.g., Wu and Emanuel 1993, 1994). This supposition is based on the quasi-horizontal nature of the 350–355 K layer (pressures vary between 175 and 200 hPa) and the observation that the winds are quasi parallel to the PV contours (compare Figs. 3j–l), rendering a simple advective explanation for the PV decrease unlikely. The combination of the long jet tail across coastal Texas and the increasing outflow poleward of Opal is manifest in the development of split flow aloft, and associated deformation, over the northwest Gulf of Mexico.

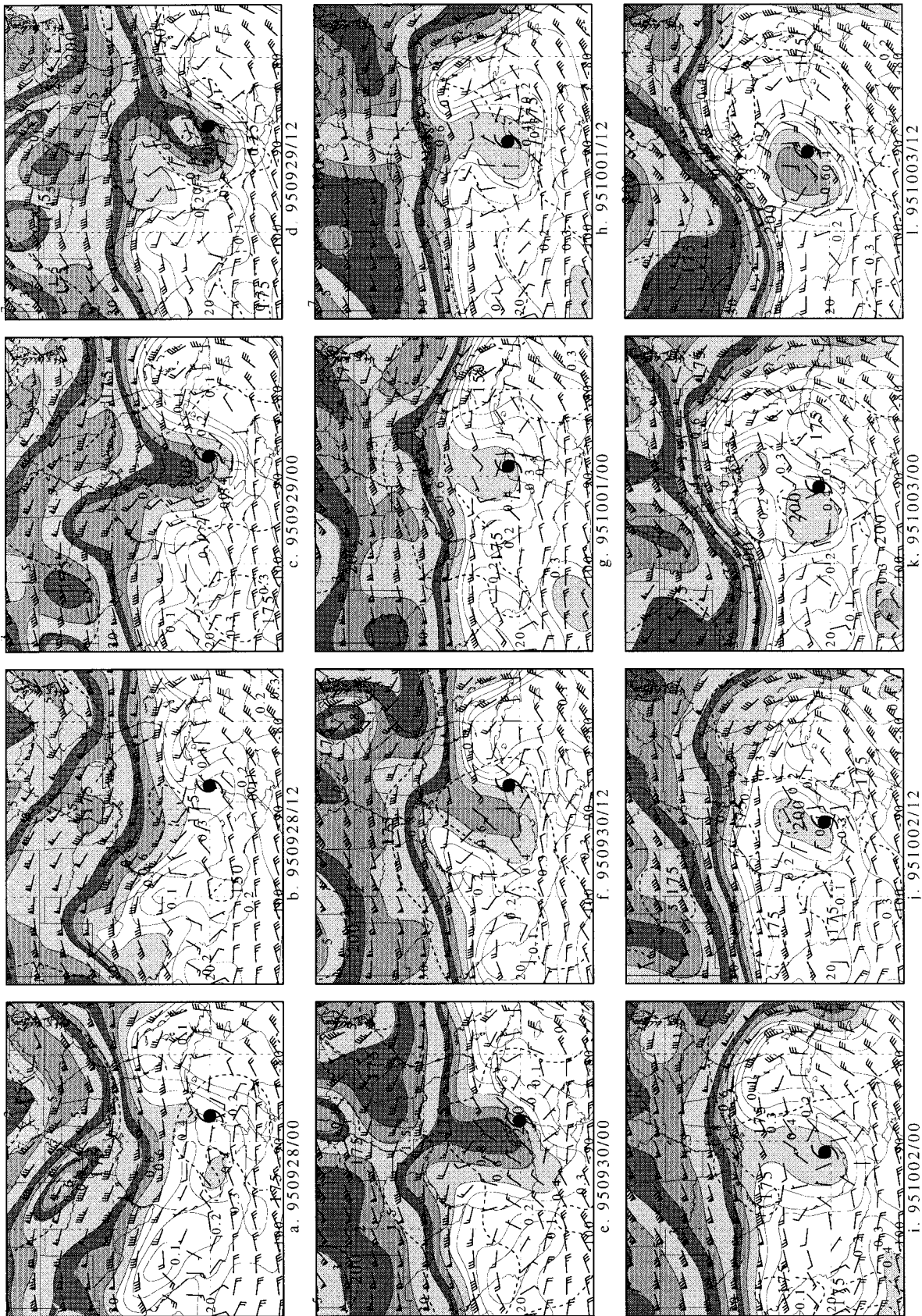


FIG. 3. The 350–355 K layer-averaged PV, pressure, and winds at 0000 UTC 28 Sep–1200 UTC 3 Oct 1995 every 12 h (a–l). Potential vorticity contours drawn every 0.1 PVU (1 PVU = $1.0 \times 10^{-6} \text{ K kg}^{-1} \text{ m}^2 \text{ s}^{-1}$), through 0.4 PVU, every 0.2 PVU through 1.0 PV, and then 1.5, 2, 3, 5, 7, 9 PVU (shading begins at 0.4 PVU). Pressures (dashed) are drawn every 25 hPa. Winds plotted in conventional wind barb format with one pennant, full barb, and half-barb denoting 25 m s^{-1} , 5 m s^{-1} , and 2.5 m s^{-1} , respectively. Location of Opal is indicated by the conventional hurricane symbol.

The rapid intensification phase of Opal is concentrated between 1800 UTC 3 October and 1000 UTC 4 October, during which time the storm deepens 47 hPa to 916 hPa (intensifying at one point at a rate of 9 hPa h^{-1} ; Figs. 2a,b). Two prominent sustained wind speed increases are observed, the first near 0000 UTC 4 October when the winds increase to 52 m s^{-1} and the second near 1000 UTC 4 October when the winds increase to 68 m s^{-1} . Landfall, defined by the time gale-force winds cross the coast, is near 0900 UTC 4 October. The eye crosses the coast near 2000 UTC 4 October whereupon rapid weakening ensues and by 0000 UTC 5 October Opal's central pressure increases to 950 hPa and maximum sustained winds decrease to 40 m s^{-1} . Although Opal is also of considerable interest because of the demonstrated positive impact of oceanic heat fluxes associated with the WCE on the rapid intensification phase (Shay et al. 2000; Black and Shay 1998), and the multiscale aspects of its pregenesis and initial development (Bracken and Bosart 1998), this paper will focus on the interactions described in the previous paragraphs during the rapid intensification phase. Other key aspects of Opal's life cycle will be discussed as required.

3. Data and analysis methodology

a. GOES winds processing

Tropospheric motions can be computed from sequential Geostationary Observational Environmental Satellite (GOES) multichannel imagery using automated techniques developed at the University of Wisconsin's Cooperative Institute for Meteorological Satellite Studies. High-density (resolution) wind vector fields can be derived from cloud and water vapor motions by taking advantage of the improved radiometric observations from the National Oceanic and Atmospheric Administration's (NOAA) latest generation of geostationary satellites, *GOES-8*. Coupled with a processing strategy aimed at optimizing the extraction of high-quality wind vectors from multiple *GOES-8* channels [infrared (IR), WV, and visible (VIS)], spatially complete and coherent wind vector fields representing upper-tropospheric flow can be achieved (Velden et al. 1998).

The traditional problem with satellite-derived wind vectors was the lack of information in regions void of cloud tracers. This problem has been alleviated in the upper troposphere with the development of WV-tracked winds (Velden et al. 1997). The *GOES-8* WV channels (one on the imager and two on the sounder) sense emissions from WV in the mid- to upper troposphere. These radiances can be converted into imagery, and selected spatial discontinuities (targets) are then tracked over intervals of 30 min to obtain motion vectors. While these vectors represent layer-mean motions in most cases, the vector height can be approximated by a combination of radiometric signal and fit to other multivariate information. Additional information on the target-

ing, tracking, height assignment, and quality control procedures can be found in Velden et al. (1997, 1998).

b. Recursive filter analysis method

A high-resolution, three-dimensional analysis procedure applied to the satellite-derived winds was used to produce wind analyses and derived diagnostic fields. This procedure is an adaptation of the recursive filter (RF) described by Hayden and Purser (1988). It is a basic successive approximation method but contains a unique feature of locally varying scaling, which gives it a greater flexibility over nonhomogeneous data. The general properties of the RF are given in Hayden and Purser (1995) and the adaptation to the satellite winds is described in Velden et al. (1998). The RF analyses are constructed at a 1.0° (~ 111 km) horizontal resolution at mandatory pressure levels and the NCEP global model analyses are employed as background fields for the RF analyses.

c. SSM/I datasets

The evolution of the convective structure of Opal was diagnosed with the use of Special Sensor Microwave Imager (SSM/I) 85-GHz imagery. The 85-GHz frequency is especially sensitive to ice crystal concentrations in the temperature range from -2° to -10°C , or about the 500–400-hPa level in hurricanes (J. D. Hawkins 1998, personal communication). These ice crystal concentration regions are highly correlated with rain below the freezing level. High spatial resolution due to the high frequency is possible with the SSM/I sensor (~ 12 km). This makes it possible to detect convective features on the scale of hurricane rainbands and eyewalls. The resulting images are similar to radar reflectivity images within hurricanes. These images frequently allow eye detection in a tropical cyclone long before it is evident in the IR or VIS imagery from GOES satellites (Velden et al. 1989).

The SSM/I images used in this study were specially processed by the Naval Research Laboratory to a storm-centered image resolution (effective) of 3 km using the methods of Poe (1990) and Hawkins et al. (1995). Discussions on the use of this type of image processing for tropical cyclone intensity estimation can be found in Hawkins et al. (1998). With four Defense Meteorological Satellite Program satellites containing SSM/I capability operating in morning and evening pairs (two satellites flying over the same area with 2–3 h separation), enough images were obtained over Opal to allow a day-to-day diagnosis of the evolution of the hurricane eyewall and rainband features.

d. TOPEX/Poseidon datasets

The TOPEX/Poseidon satellite is designed to measure sea height anomaly (SHA) through use of a dual-fre-

quency, KU-band microwave altimeter, which detects deviations from the mean geoid with an accuracy of 2 cm or less using distortions in the leading edge of the radar pulse. Atmospheric moisture attenuation is measured directly and used to remove errors in the SHA. A mean geoid has been computed over precise ground tracks over the world's oceans, which vary less than 1 km between repeat orbits. The repeat period is 10 days. The mean geoid climatology for the Gulf of Mexico region is computed over the time period from 1992 to 1995. Repeat tracks are separated by 315 km, or about 3.0° long.

Due to differences in subsurface ocean density, variations in sea height of the order of tens of centimeters can occur over ocean features such as the Gulf Stream and LC as well as over associated oceanic eddy circulations. The power of TOPEX lies in its ability to detect these important ocean circulations irrespective of atmospheric moisture variations and ocean surface thermal signatures. This is especially important in the summer in the Gulf of Mexico where a thin, uniform, warm mixed layer develops in response to strong insolation. Important circulation features in the Gulf of Mexico, which are easily viewed during fall, winter, and spring by polar-orbiting Advanced Very High Resolution Radiometer (AVHRR) satellite sensors, are not easily visible in the summer. Instead, the Gulf of Mexico appears as a nearly uniform water body from a surface SST point of view until the water is disturbed by strong winds, which eliminate the thin, warm mixed layer.

The 10-day repeat values of SHA were objectively analyzed and interpolation was performed in the regions of no data between the repeat orbits (separation distance of 315 km). A new method, introduced by Goni et al. (1997), was used by Shay et al. (2000) to estimate the heat content of the upper ocean over the Gulf of Mexico before and after Opal. They showed large heat content changes occurred over the LC eddy where SSTs remained almost unchanged as heat was extracted from the water column. In adjacent areas of shallow, warm mixed layers, large SST changes resulted in relatively little heat flux into the storm.

4. Results

This section begins with a presentation of the high-density *GOES-8* WV winds to depict the important synoptic and subsynoptic-scale circulation features in the Opal environment. It is followed by an analysis of the layer-mean (300–200 hPa) divergence, 6-h layer-mean divergence change, and layer-mean vorticity to support our contention that a trough–jet–hurricane interaction was important to the rapid intensification phase of Opal. It concludes with an analysis of satellite and aircraft observations, oceanic influences, and a quantitative analysis of the trough–jet–hurricane interaction from a calculation of Eliassen's (1952) balanced vortex (BV)

radial-vertical circulation as modified by Molinari and Vollaro (1990).

a. Upper-tropospheric environmental flow analysis

GOES-8 WV wind plots centered at 2345 UTC 2 October and 1145 UTC 3 October are shown in Figs. 4a,b (datasets for 0600 UTC are not available due to image blackouts from satellite eclipse). Similar plots for 1745 UTC 3 October and 2345 UTC 3 October are presented in Figs. 5a,b. Collectively, Figs. 4 and 5 demonstrate the extensive areal coverage and excellent spatial coherence of the WV winds. The winds are plotted over three pressure layers using the procedures described in section 3a.

At 2345 UTC 2 October (Fig. 4a), a time when Opal has a central pressure near 970 hPa and maximum sustained winds near 35 m s^{-1} (Fig. 1), the large-scale flow pattern is characterized by a broad west-southwesterly airflow over the southeastern United States, a ridge over the Gulf of Mexico, and a northerly outflow channel over the northwestern Caribbean. A meridionally oriented trough near 100°W extends equatorward into southwestern Texas and extreme northeastern Mexico. Within this trough there is evidence for a smaller-scale trough extension over extreme southern Texas. The winds west of Opal, although fewer in number, suggest the presence of a deformation region. Opal is well south of the jet-entrance region over the southern United States at this time.

By 1145 UTC 3 October (Fig. 4b) the northerly outflow channel curving to the east of Opal strengthens, the flow becomes more anticyclonic over the southeastern United States, and the trough over the central United States acquires a slight positive tilt (northeast–southwest). This positive trough tilt arises because the equatorward end of the trough stalls near the southern tip of Texas where the smaller-scale trough extension is readily apparent (recall also the discussion of Fig. 31). This flow configuration can be one possible early signature of trough fracture. A trough that elongates meridionally in a deformation region may eventually split (fracture) as the equatorward end of the trough starts to lag behind the more rapidly moving part of the trough that lies more poleward (see, e.g., Dean and Bosart 1996).

Upstream of the smaller-scale trough over coastal southern Texas the flow bifurcates. One branch turns northeastward across extreme southern Texas while another branch curves southeastward and appears to move around the equatorward side of Opal. Immediately west of Opal the WV winds suggest the existence of a meridionally oriented shear line and trough. This feature is consistent with the NCEP initialized analysis of an intensifying smaller-scale PV anomaly near Opal (Fig. 31). Meanwhile, the combination of increasing anticyclonic flow over the southeastern United States and the development of a positive tilt to the upstream trough

over the Midwest has also impacted the jet poleward of Opal. The winds in this jet back to more southwesterly near 30°N and 95°W as Opal starts to accelerate to the northeast.

By 1745 UTC 3 October (Fig. 5a) the flow aloft has become even more anticyclonic over the southeastern United States, a strong outflow channel continues to the north and east of Opal, and winds in the jet-entrance region continue to back and are now from the south-southwest. The smaller-scale trough identified near the southern tip of Texas at 1145 UTC 3 October (Fig. 4b) has moved to a position over the extreme northwestern Gulf of Mexico. It can be identified by the cyclonic curvature in the southwesterly flow in the 251–350-hPa layer over the water and by the north-northwesterly flow in the 351–500-hPa layer over the adjacent land. Although not a classic trough fracture of the type discussed by Dean and Bosart (1996), this smaller-scale trough is lagging behind from the more progressive poleward part of the larger-scale trough.

At 2345 UTC 3 October (Fig. 5b) the jet poleward of the now rapidly intensifying Opal (central pressure near 955 hPa and peak winds near 50 m s^{-1}) is well defined. The jet corridor is sandwiched between the ridge along the Atlantic coast and the slow eastward-moving, positively tilted midwestern trough. Winds in the jet corridor exceed 50 m s^{-1} and the area of winds greater than 25 m s^{-1} in the jet entrance region extend southwest toward coastal Louisiana. Although it is now difficult to distinguish the earlier smaller-scale troughs over the extreme northwestern Gulf and near Opal, the WV winds still suggest that the flow is cyclonic in these areas. Subsequent to 0000 UTC 4 October Opal continues to strengthen as it approaches the jet-entrance region while crossing the WCE. Weakening commences just after 1000 UTC 4 October as the storm exits the WCE region and continues through landfall (eye) at 2000 UTC 4 October at which time the shear over the storm is increasing rapidly (discussed more fully in section 4e).

b. Upper-tropospheric diagnostics

This section shows the layer-averaged (300–200 hPa) divergence, deformation, and absolute vorticity constructed from the three-dimensional recursive filter analysis procedure applied to the satellite-derived winds as outlined in section 3b. These layer-averaged fields were constructed for the period 0000 UTC 3–5 October at 6-h intervals (except for 0600 UTC when the satellite was in eclipse). Analyses of the 6-h change in the divergence fields were also prepared. These fields will be used to help diagnose the evolution of the interaction between Opal and the upper-tropospheric features described in the previous section.

At 0000 UTC 3 October the maximum divergence near Opal is situated to the southeast of the storm in the strong outflow channel there (Figs. 6a,b). Another

area of divergence exists along the Gulf coast and extends back to southern Texas along an axis of higher wind speeds ($25\text{--}30 \text{ m s}^{-1}$). A local maximum in resultant deformation is seen near coastal southern Texas. The meridional orientation of the axes of dilatation in this region is consistent with the development of flow bifurcation by 1200 UTC 3 October (Figs. 3l and 4b) over coastal northeastern Mexico and southeastern Texas. An area of estimated strong cyclonic vorticity advection (CVA) centered over eastern Texas marks the advancing southern extension of the trough (Fig. 6c).

By 1200 UTC 3 October the divergence associated with the anticyclonic shear side of the jet-entrance region expands equatorward toward Opal (Figs. 6d,e). An area of weak CVA over coastal southeastern Texas marks the lagging equatorward end of the Midwest trough (Fig. 6f). A deformation maximum persists over the extreme northwestern Gulf of Mexico and along the southeast coast of Texas (Fig. 6a). The continuing meridional orientation of the axes of dilatation in this area favors the strengthening flow bifurcation to the west and north of Opal discussed previously (Figs. 3l, 4b, 6a). The tendency for the flow to stretch meridionally to the northwest of Opal is also consistent with the lagging equatorward end of the Midwest trough. Note also the weak downstream ridging offshore of Louisiana as Opal begins to interact with the jet and trough (Fig. 6f).

At 1800 UTC 3 October, just prior to the onset of rapid intensification, the divergence (values in excess of $3.0 \times 10^{-5} \text{ s}^{-1}$) associated with the trough and jet-entrance region continues to elongate southwestward toward Opal (Figs. 7a,b). In effect, the divergence associated with the smaller-scale troughs over the northwestern Gulf and near Opal is becoming linked to the southwestern end of the elongated divergence axis associated with the jet-entrance region. The continuing persistent deformation and meridional orientation of the axes of dilatation over the northwestern Gulf favors the elongation of the smaller-scale trough along the Texas coast toward Opal (Fig. 7a). One result of this process is the establishment of a northwest–southeast-oriented axis of absolute vorticity from Texas toward Opal (Fig. 7c). Weak ridging over southeastern Louisiana also helps to delineate the elongated smaller-scale trough as winds become more southerly in the outflow region poleward of Opal (Fig. 7a).

Strong divergence maxima are situated over Tennessee and equatorward of Louisiana, respectively, at 0000 UTC 4 October (Figs. 7d,e). The northern maximum lies downstream of an area of estimated CVA and marks the principal jet-entrance region (Figs. 7d,e). The southern maximum, little changed in intensity from 1800 UTC 3 October, overlaps the poleward side of Opal. It continues to be associated with the remnant smaller-scale trough over the northwest Gulf of Mexico and a second distinct entrance region associated with the jet tail (Fig. 7d).

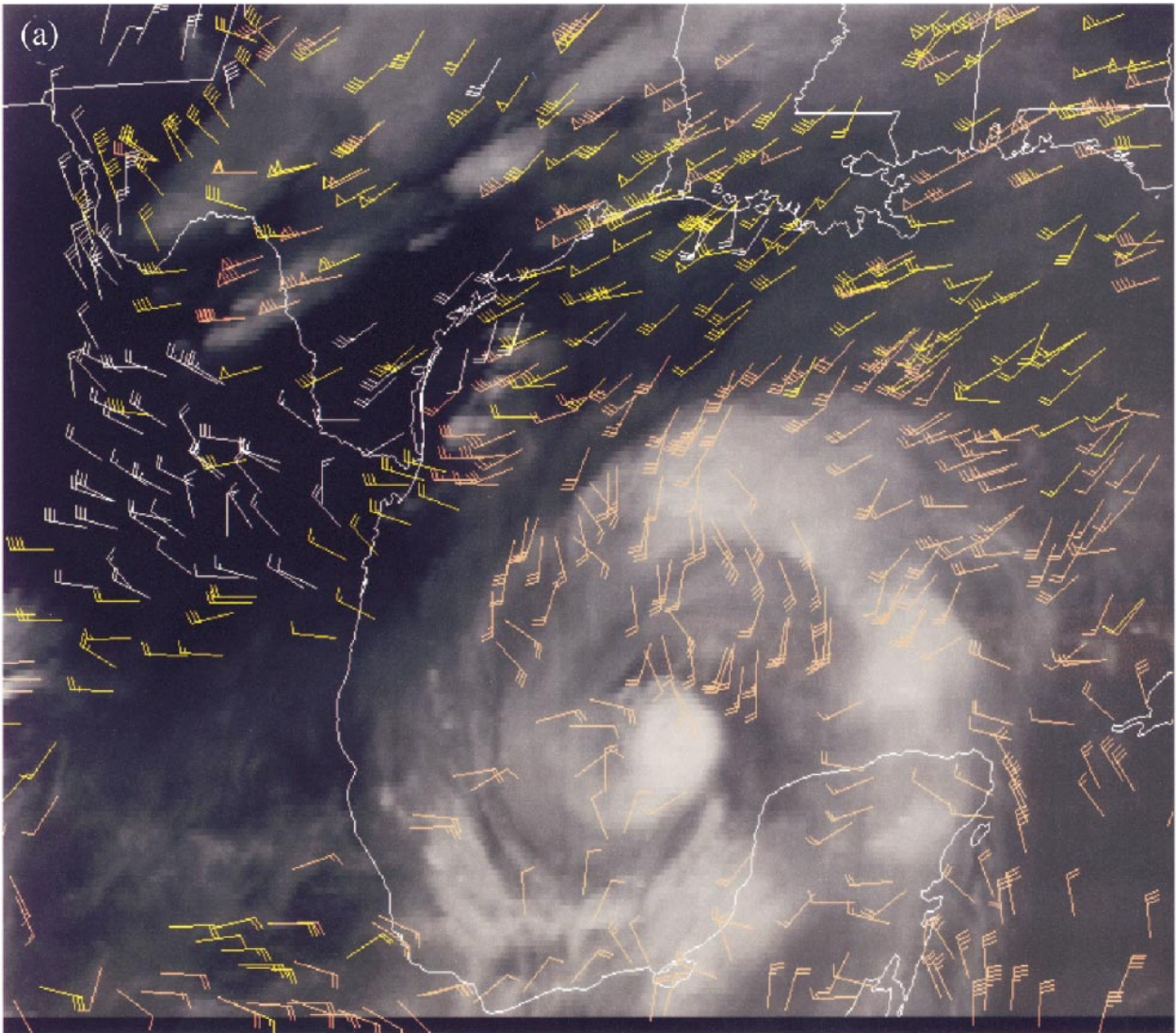


FIG. 4. High-density *GOES-8* water vapor (WV) winds superimposed over the WV imagery for (a) 2345 UTC 2 Oct 1995 and (b) 1145 UTC 3 Oct 1995. Winds plotted as in Fig. 3. Pressure scale for the color-coded winds (salmon: 150–250 hPa, yellow: 251–350 hPa, and white: 351–500 hPa).

As Opal approaches the coast by 1200 UTC 4 October the divergence maximum just poleward of the storm strengthens (Fig. 8b). This divergence maximum, situated over extreme southeastern Louisiana, is collocated with a very distinct second jet-entrance region on the eastern edge of a deformation maximum (Figs. 8a,b). The development of an absolute vorticity minimum over Alabama where the outflow from Opal reaches the jet-entrance region ensures the growth of a prominent region of (estimated) CVA poleward of Opal (Fig. 8c). Only a remnant of the smaller-scale Texas trough can be seen near coastal southeastern Louisiana at this time (Fig. 8c). By 1800 UTC 4 October the southern divergence maximum intensifies, retreats farther onshore, and is associated with a well-defined area of CVA (Fig. 8e) as Opal continues to weaken.

A comparison of the divergence analyses for 0000 UTC 3 October and 1200 UTC 3 October (Figs. 6b and 6e) shows that the largest positive divergence change (increasing divergence) is concentrated along the Gulf coast as Opal began to accelerate northeastward. By 1800 UTC 3 October (Fig. 7b), however, the area of positive 6-h divergence change (shown shaded) has overspread the poleward side of Opal (peak value in excess of $2.5 \times 10^{-5} \text{ s}^{-1}$) in conjunction with the superposition of the jet-entrance region and the approach of the smaller-scale trough over the extreme northwestern Gulf of Mexico (Figs. 5a and 7b). This large area of positive divergence change near Opal just prior to the onset of rapid intensification (~ 2100 UTC 3 October) suggests that upper-level dynamical processes are playing an important role in the initiation of the inten-

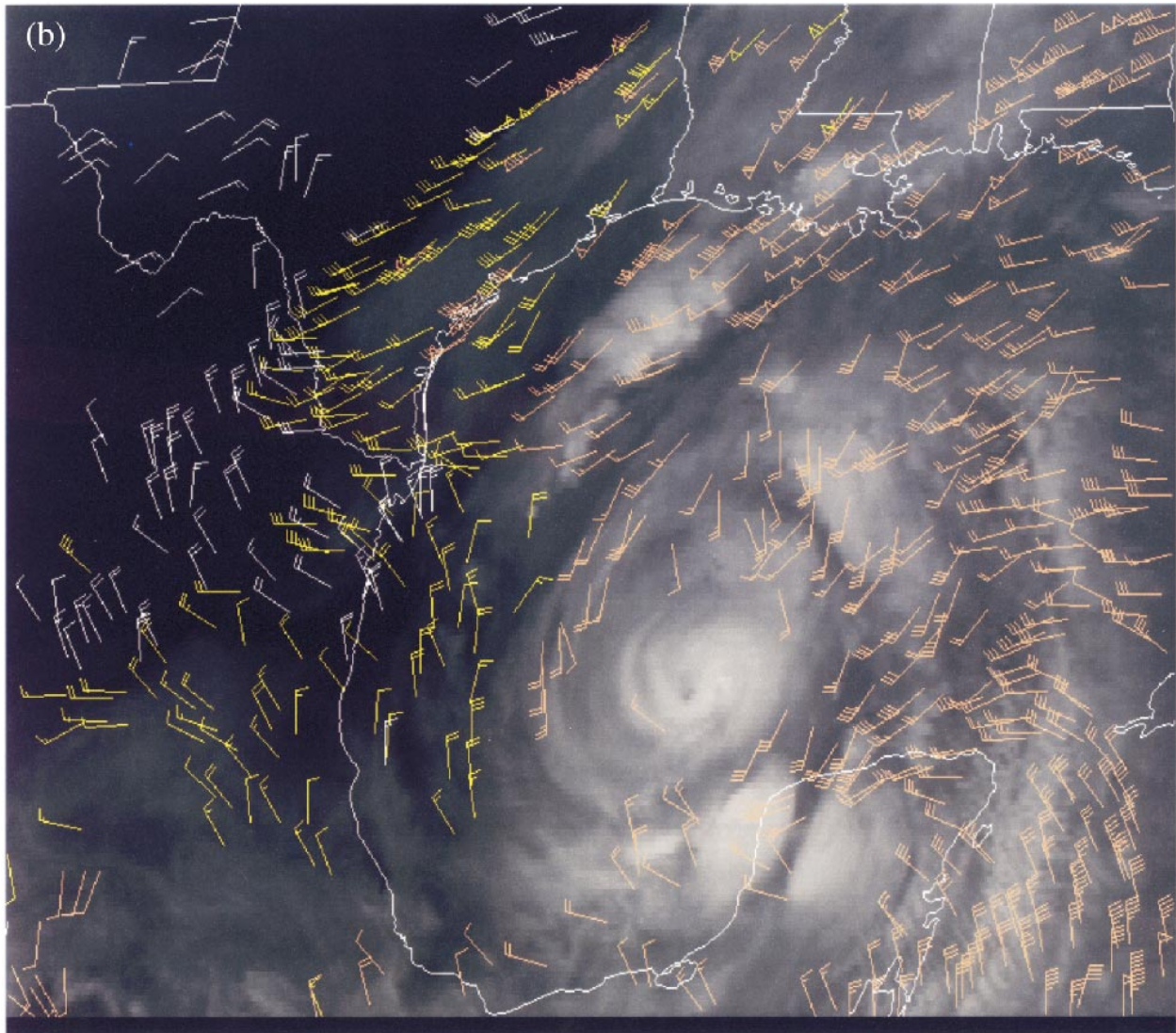


FIG. 4. (Continued)

sification process. Also, the apparent hurricane–trough–jet dynamical interaction is occurring ~ 6 h before Opal’s eye reaches the WCE, a source of enhanced oceanic heat and moisture fluxes into the storm (Shay et al. 2000).

At 0000 UTC 4 October the growth of divergence had lessened, although there still is an area of positive divergence change (6 h) near and to the northwest of Opal (Fig. 7e). Little change in intensity or position of the divergence center poleward of Opal is seen by 1200 UTC 4 October (Fig. 8b; absence of a 0600 UTC image precludes a 6-h divergence change calculation). By 1800 UTC 4 October, at which time Opal is weakening rapidly before the eye crosses the coast, the region of positive divergence change is centered well to the northeast of Opal in the jet-entrance region (Fig. 8e). The peak positive 300–200-hPa divergence change at 1800 UTC 4

October exceeds $6.0 \times 10^{-5} \text{ s}^{-1}$ in the strong southwesterly flow ahead of the advancing trough (Fig. 8e). This divergence-change signature and associated divergence pattern is consistent with a decaying tropical storm accelerating poleward into stronger midlatitude westerlies.

c. Satellite and aircraft signatures

This section begins with a large-scale overview based on a sequence of WV images for 2315 UTC 2 October, 1115 UTC and 2315 UTC 3 October, and 1115 UTC 4 October shown in Figs. 9a–d, respectively. The WV image for 2315 UTC 2 October clearly shows the signature of the large-scale trough and jet that extends from the southwest across Texas well to the northwest of Opal (Fig. 9a). Over the next 12 h the trough moves eastward

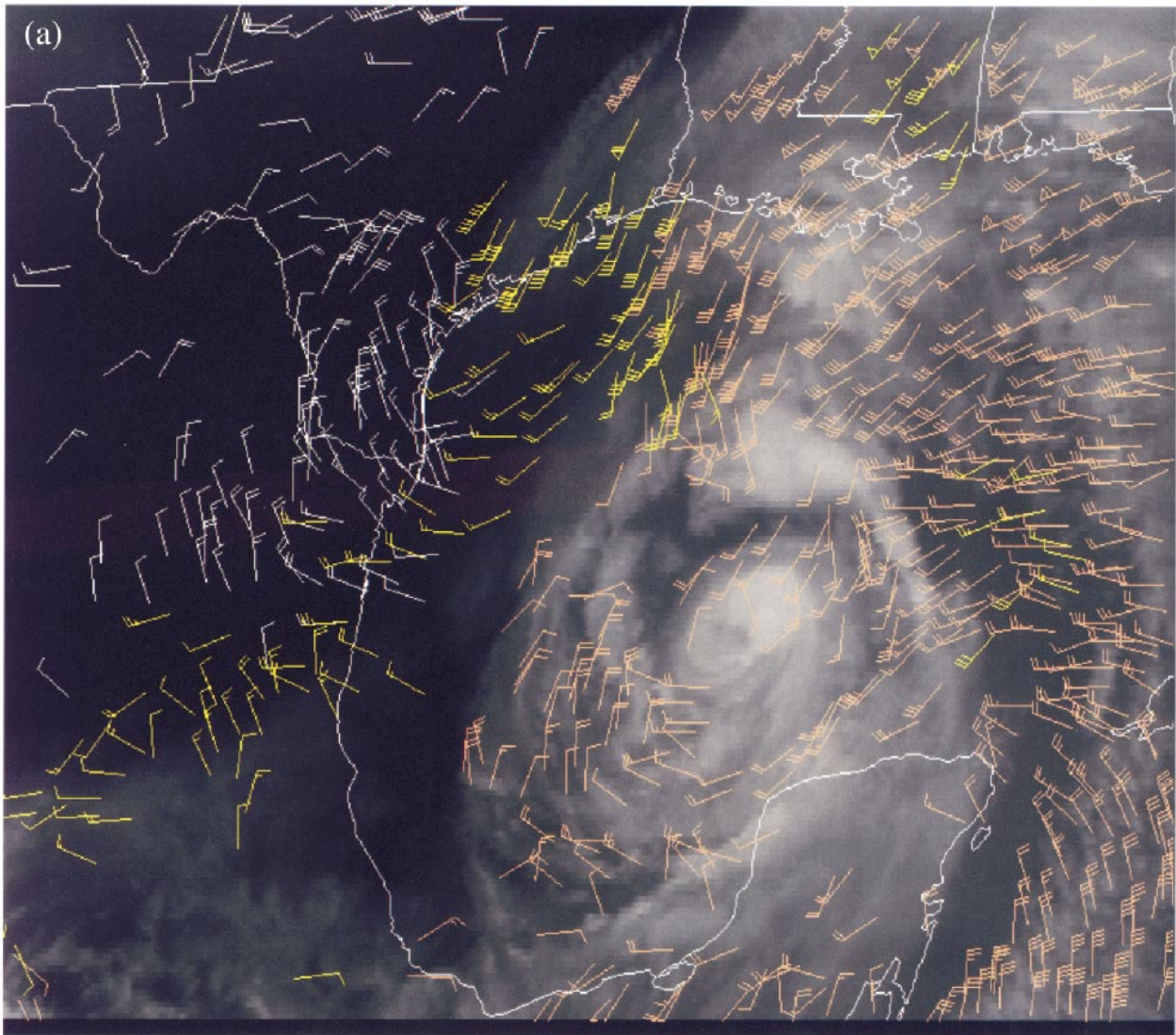


FIG. 5. As in Fig. 4 except for (a) 1745 UTC and (b) 2345 UTC 3 Oct 1995.

in midlatitudes while the trough tail lags behind somewhat as it extends southwestward into extreme southeastern Texas and northeastern Mexico (Fig. 9b). As the equatorward end of the trough approaches Opal there is evidence for the development of an area of convection poleward of Opal along the leading edge of the moist band by 1115 UTC 3 October (Fig. 9b). By 2315 UTC 3 October, and continuing through 1115 UTC 4 October, the area of convection over the Gulf poleward of Opal expands significantly as the moist outflow into the jet-entrance region develops a classic anticyclonic curvature signature (Figs. 9c,d). Drier air at mid- and upper-tropospheric levels reaches the extreme northwestern Gulf by 2315 UTC 3 October and fully envelops the west side of Opal by 1115 UTC 4 October (Figs. 9c,d).

An analysis of SSM/I imagery and reconnaissance aircraft flight-level wind data are next used to show

whether the intensification of Opal can be associated with an eyewall replacement cycle and/or an eyewall contraction. SSM/I imagery for available time periods during Opal's intensification are presented in Fig. 10. From 0042 UTC through 1619 UTC 3 October the majority of the deep convection (yellow and red areas) lies equatorward and to the southeast of Opal. Between 2344 UTC 3 October and 0030 UTC 4 October the eye becomes encircled by deep convection and almost closes off. Comparison with Fig. 2b shows that the measured sustained winds increased rapidly from 38 to 52 m s^{-1} near 0000 UTC 4 October at the time Opal's eye almost closes off. Although areas of deep convection poleward and to the west of Opal appear to wrap cyclonically around the storm at distances of 200–300 km from the center while exhibiting a tendency to move inward during the 12 h ending 0337 UTC 4 October, there is no

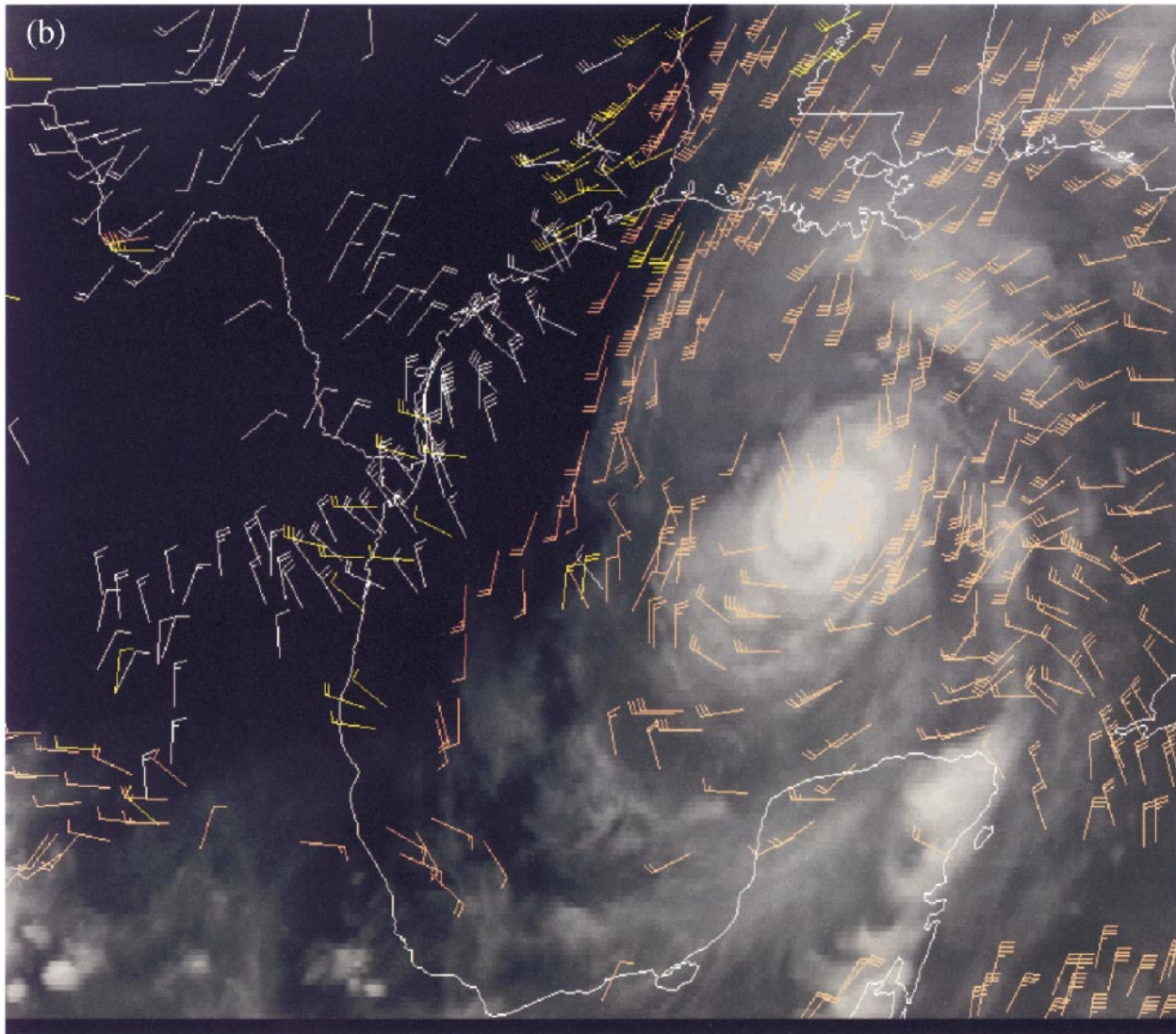


FIG. 5. (Continued)

persuasive evidence in the SSM/I imagery for the presence of an eyewall replacement cycle during the rapid intensification phase of Opal. In subsequent times (0337 UTC 3 October–1566 UTC 4 October) there is a general increase in the areal extent of deep convection, especially poleward of Opal (see also Figs. 9c,d), as the storm reaches peak intensity and then begins to weaken. The expansion of deep convection poleward of the storm is consistent with the divergence, vorticity, and CVA patterns shown in Figs. 7a–f, 8a–c. It also appears that the eyewall contracts between 2344 UTC 3 October and 2140 UTC 4 October in the SSM/I imagery (Fig. 10), consistent with the contracting radius of maximum wind shown in Fig. 2b. Finally, an IR image for 0815 UTC 4 October near the time of Opal's peak intensity is shown in Fig. 11. This IR image suggests the presence

of a band of deep convection wrapping cyclonically around the equatorward side of the now very distinct eye (a scenario suggested in the available SSM/I imagery despite the gap between 0337 UTC and 1214 UTC 4 October in Fig. 10) along with a separate area of deep convection poleward of Opal (also consistent with the available SSM/I imagery.)

Reconnaissance aircraft from the U.S. Air Force monitored Opal nearly continuously while the storm was over the Gulf of Mexico. U.S. Air Force planes generally flew north–south and east–west tracks through Opal at different flight levels. Reconnaissance aircraft flight-level winds, available at a spacing of ~ 500 m, are displayed in time-distance cross section format within 150 km of the storm center for north–south (Fig. 12; left) and east–west (Fig. 12; right) passes within 150

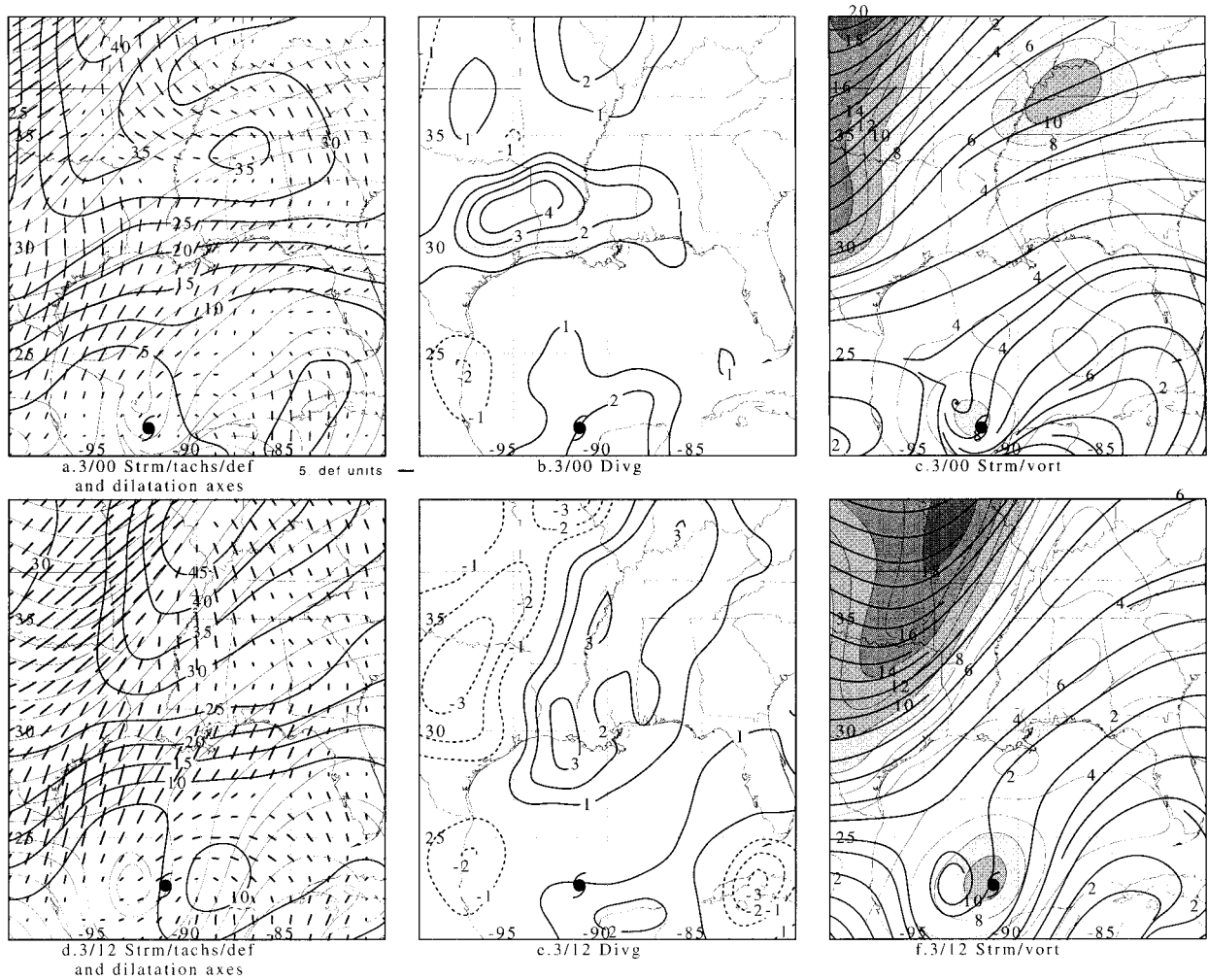


FIG. 6. The 0000 UTC 3 Oct 1995 fields. (a) The 300–200-hPa layer-mean streamlines (thin solid) and isotachs (heavy solid; every 5 m s^{-1}). Magnitude of resultant deformation and orientation of the axis of dilatation indicated by bold line segments (scale at lower right indicates five deformation units where 1 unit equals $1 \times 10^{-5} \text{ s}^{-1}$). (b) The 300–200-hPa layer-mean divergence (contoured every $1 \times 10^{-5} \text{ s}^{-1}$) with the zero contour omitted. Solid (dashed) contours denote divergence (convergence), respectively. (c) The 300–200-hPa layer-mean streamlines (heavy solid) and absolute vorticity (thin solid every $2 \times 10^{-5} \text{ s}^{-1}$; shading begins at $8 \times 10^{-5} \text{ s}^{-1}$). (d)–(f) As in (a)–(c) except for 1200 UTC 3 Oct 1995. Location of Opal is denoted by the conventional hurricane symbol in all panels.

km of the storm center. The two data gaps in these plots occur where the aircraft changed flight level, first from ~ 900 to 850 hPa , and second from ~ 850 to 700 hPa .

Slow storm intensification in the 12 h ending 0600 UTC 3 October is associated with an increase of eyewall winds to $35\text{--}40 \text{ m s}^{-1}$, primarily on the equatorward and eastern flank of the storm. Rapid intensification in the 15 h ending 0900 UTC 4 October accompanies an eyewall contraction as the strongest winds ($\sim 60 \text{ m s}^{-1}$) shift to the poleward and western flank of the storm. The results from Fig. 12 suggest that there appears to be an association between the eyewall contraction and storm intensification. However, in support of the SSM/I imagery results there is no definitive evidence from the reconnaissance aircraft data for a classical eyewall replacement (Willoughby et al. 1982; Willoughby 1990) before or during the rapid intensification. This inter-

pretation is bolstered by reexamining the U.S. Air Force reconnaissance measurements displayed in Figs. 2a,b. The time history of the radius of maximum wind shows no evidence for an eyewall replacement cycle during the rapid intensification. The decrease in the radius of maximum winds follows the decrease in minimum central pressure and the increase of the primary (eyewall) wind maximum. Accordingly, the decrease of the radius of maximum winds may be more a consequence of intensification rather than a cause of it.

However, Fig. 12 does indicate evidence for an eyewall replacement cycle after the rapid intensification has ended as judged by the 700-hPa secondary wind maximum ($35\text{--}45 \text{ m s}^{-1}$) roughly 100 km from the center near 1200 UTC 4 October. There is also some evidence for enhanced convection roughly 100 km poleward of the storm center in the SSM/I imagery for 1214 UTC

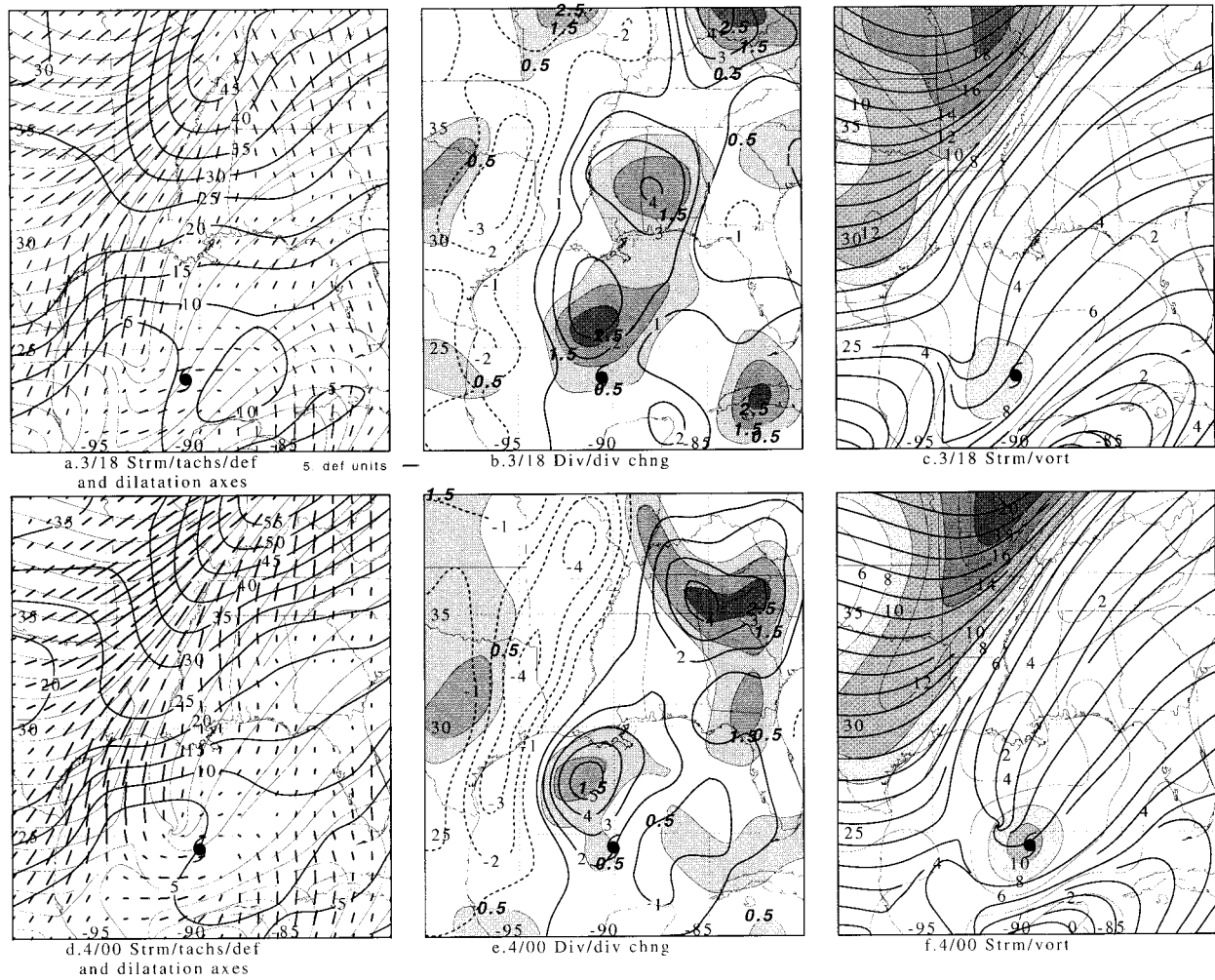


FIG. 7. As in Fig. 6 except for 1800 UTC 3 Oct 1995 (a)–(c) and 0000 UTC 4 Oct 1995 (d)–(f). In (b) and (e) the change in the layer-mean 300–200-hPa divergence change over the previous 6 h is shaded for increasing values of divergence contoured every $1 \times 10^{-5} \text{ s}^{-1}$ beginning at $0.5 \times 10^{-5} \text{ s}^{-1}$.

and 1259 UTC 4 October (Fig. 10) that may also indicate a possible eyewall replacement cycle in progress. The eyewall replacement cycle likely contributed to the rapid weakening of Opal after 1200 UTC 4 October along with the increased shear and the departure of the storm from the WCE.

Velden and Olander (1998) report on a new multispectral satellite technique that delineates between regions of vigorous deep convective cloud and other cloud debris. This technique may have an application to diagnosing tropical storm intensity changes because of the important role that diabatic processes associated with active deep convection play in the storm intensity change process. The method involves the differencing of collocated GOES IRW (IR window) and WV ($6.7 \times 10^{-6} \text{ m}^{-1}$) pixel values. In most regions the IR brightness temperatures (BT) are warmer than the collocated WV BT due to radiative (absorption) properties of the respective wavelengths (i.e., the IRW is less sensitive

to atmospheric moisture and therefore this channel senses lower into the “warmer” troposphere). This situation holds for conditions of clear sky, lower-tropospheric clouds, or upper-tropospheric semitransparent clouds. In regions of upper-tropospheric opaque cloudiness, the IRW/WV BTs become virtually equal.

However, there is one condition that can result in WV radiances warmer than collocated IRW radiances. In regions of active, deep convection the WV BT can become warmer due to the presence of water vapor that has been pushed/injected into the lower stratosphere by the convective cloud tops. The WV channel absorbs radiation emitted from this water vapor and reradiates at the warmer stratospheric temperatures (Schmetz et al. 1997). The WV/IRW BT difference is greatest for cloud tops at or slightly above the tropopause (i.e., vigorous convection). In hurricanes the largest WV/IRW BT differences would be expected to be found in the region of active deep convection in the eyewall. Black (1977,

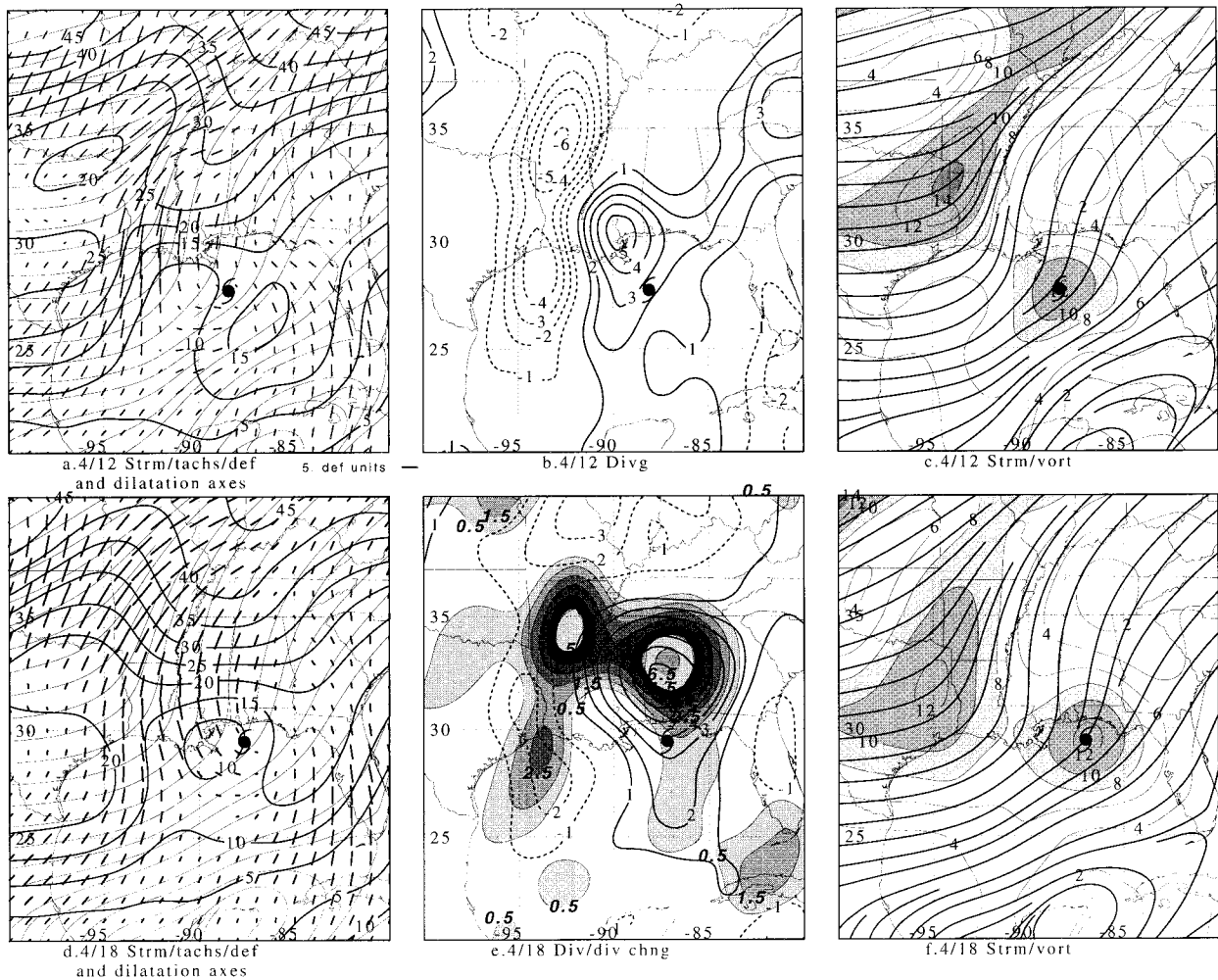


FIG. 8. As in Fig. 6 except for 1200 UTC 4 Oct 1995 (a)–(c) and 1800 UTC 4 Oct 1995 (d)–(f). In (e) the change in the layer-mean 300–200-hPa divergence change over the previous 6 h is shaded for increasing values of divergence contoured every $1 \times 10^{-5} \text{ s}^{-1}$ beginning at $0.5 \times 10^{-5} \text{ s}^{-1}$.

1983) has shown that the tropopause tends to bulge upward associated with the active deep convection in the eyewall, and there is also evidence for the penetration of the convective towers into the lower stratosphere. These active convective regions appear as warmer pixels in the WV relative to the IRW (Velden and Olander 1998). This “deep convection parameter” (hereafter DCP) method analyzes all pixels between prescribed radii (24–144 km) from the storm center, and isolates the warmer WV pixels, thereby “filtering out” the other cloud debris. The DCP trends for Opal (expressed as a count of warmer WV pixels during the intensification period) are shown in Fig. 13.

Comparison of Figs. 2a, 12, and 13 suggests that the convective burst beginning near 0800 UTC 3 October can be associated with a temporary decrease in eye radius, the onset of a steady decrease in the radius of maximum wind in the eyewall and an increase in eyewall wind speeds to 35–40 m s^{-1} . A brief storm central

pressure decrease (<5 hPa) may also be related to the 0800 UTC 3 October convective burst. Montgomery and Kallenbach (1997) and Montgomery and Enagonio (1998) have utilized highly idealized three-dimensional, quasigeostrophic (QG) numerical models to study the effects of the redistribution of convectively induced low-level PV maxima by vortex Rossby waves on early stage (nonhurricane) storm development. Storm symmetry is created by the filamentation and absorption of the convectively induced PV maxima around the developing vortex. Although these QG models may be more applicable to the initial spinup of a vortex, the theoretical results suggest that observational studies that focus on how external dynamical processes stimulate the asymmetric distribution of convection in a developing tropical storm and how the storm-scale circulation responds to the convective development could be insightful. It is conceivable that the initial convective burst near 0700–0800 UTC 3 October (Fig. 13) and observed

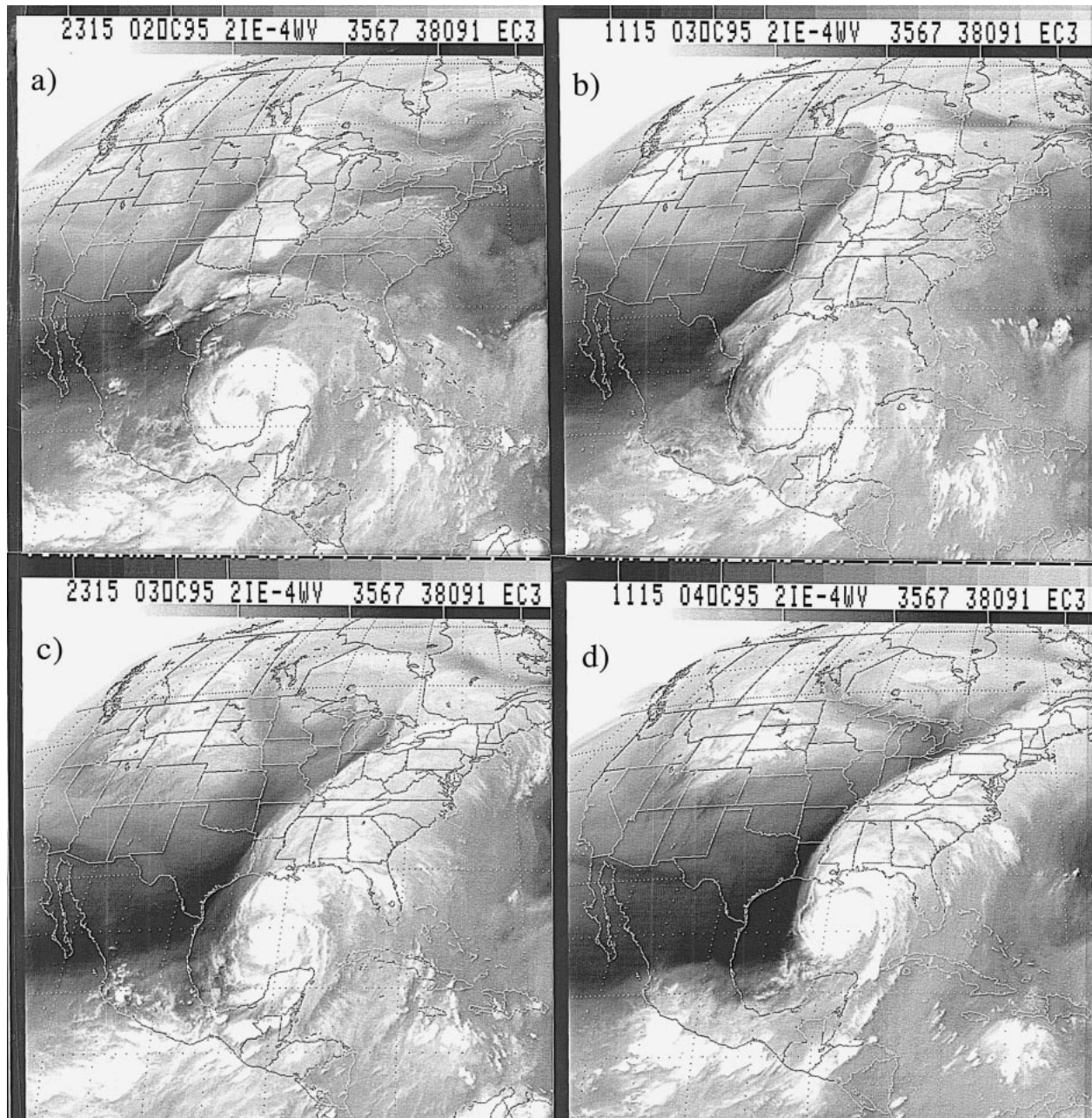
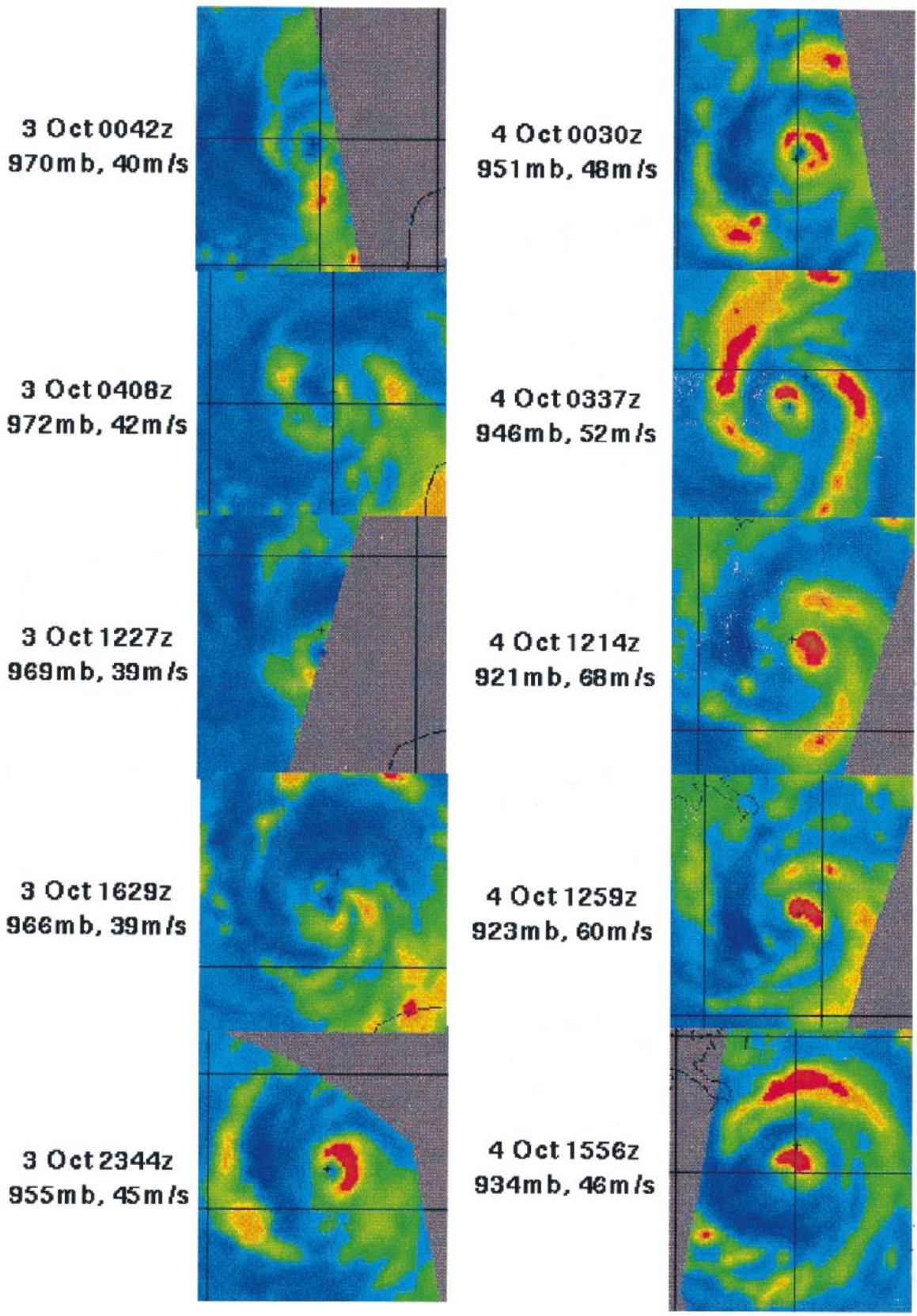


FIG. 9. GOES-8 satellite WV imagery for (a) 2315 UTC 2 Oct, (b) 1115 UTC 3 Oct, (c) 2315 UTC 3 Oct, and (d) 1115 UTC 4 Oct 1995.

eyewall wind speed maximum near 0700–0800 UTC 3 October (Fig. 12) may have perturbed the immediate storm environment sufficiently to induce a more vigorous internal dynamical response (in conjunction with mesoscale vertical motions induced by the approaching trough) in the storm core ~ 12 h later. Although data to address this issue is lacking, it is apparent from the SSM/I imagery for 0337 UTC 4 October (Fig. 10) that there was a significant increase in the extent of deep convection just to the west of Opal in the 3-h period ending at this time.

A relative convective minimum (lower bin counts) follows the initial brief convective burst from 1200 to 2000 UTC 3 October. This relative minimum in the DCP occurs at a time when the 300–200 layer-averaged divergence over and poleward of Opal increases as can be seen from a comparison of Figs. 6e and 7b. To help bolster this comparison the 300–200-hPa divergence as derived from the RF analyses, averaged over an area on the poleward side of Opal, is also displayed in Fig. 13. The divergence calculation is made over a 2 by 3 grid-point rectangular area (long axis in the zonal direction).



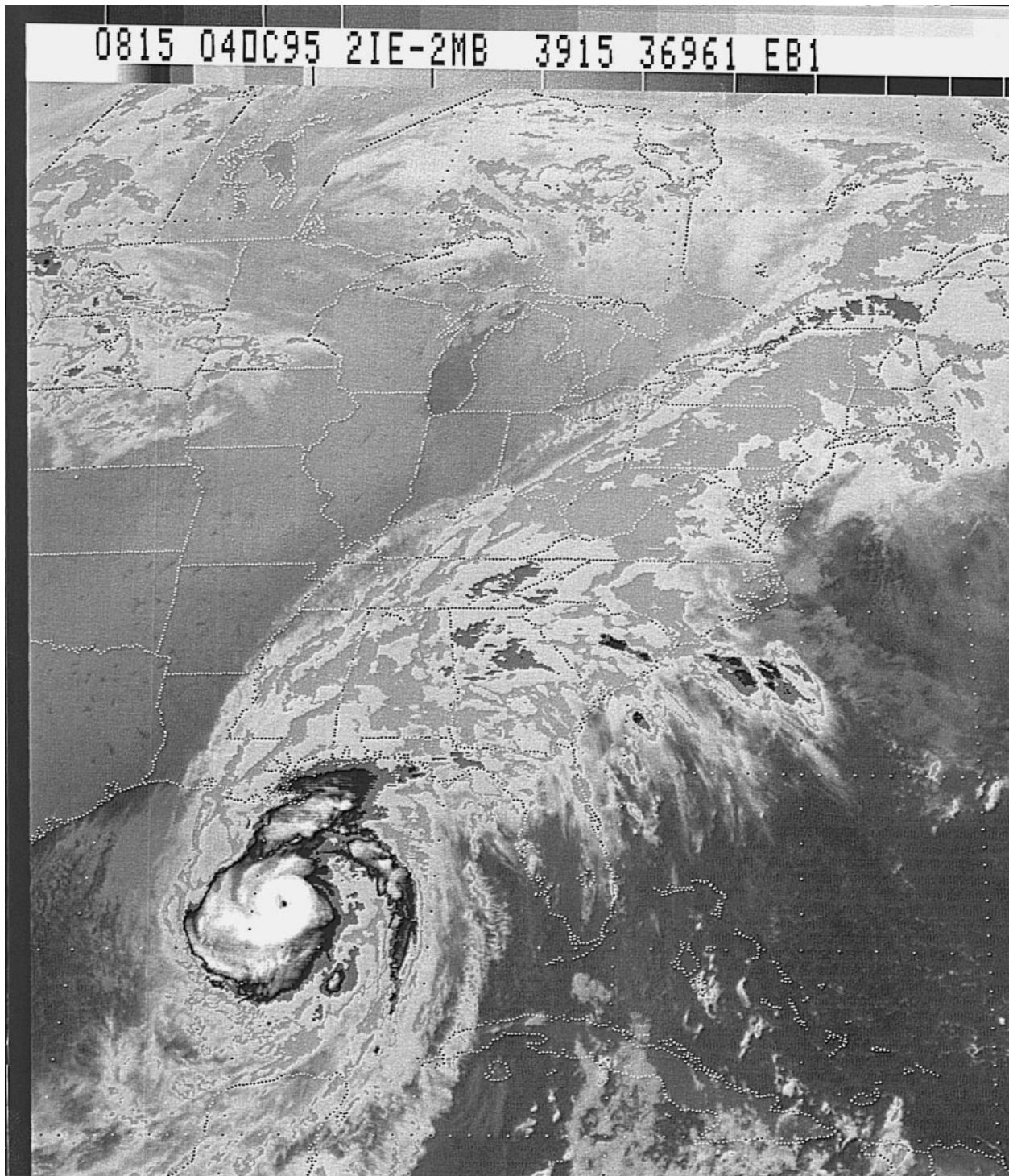


FIG. 11. Infrared (IR) *GOES*-8 satellite image for 0815 UTC 4 Oct 1995, operational MB curve enhancement.

←

FIG. 10. SSM/I satellite imagery for selected times (UTC) on 3–4 Oct 1995 as indicated to the left of each panel. Each panel is 4° (~ 450 km) on a side and is centered on Opal. Yellows and reds indicate regions of active deep convection and correspond to approximate cloud-top temperatures of -45° and -60°C , respectively.

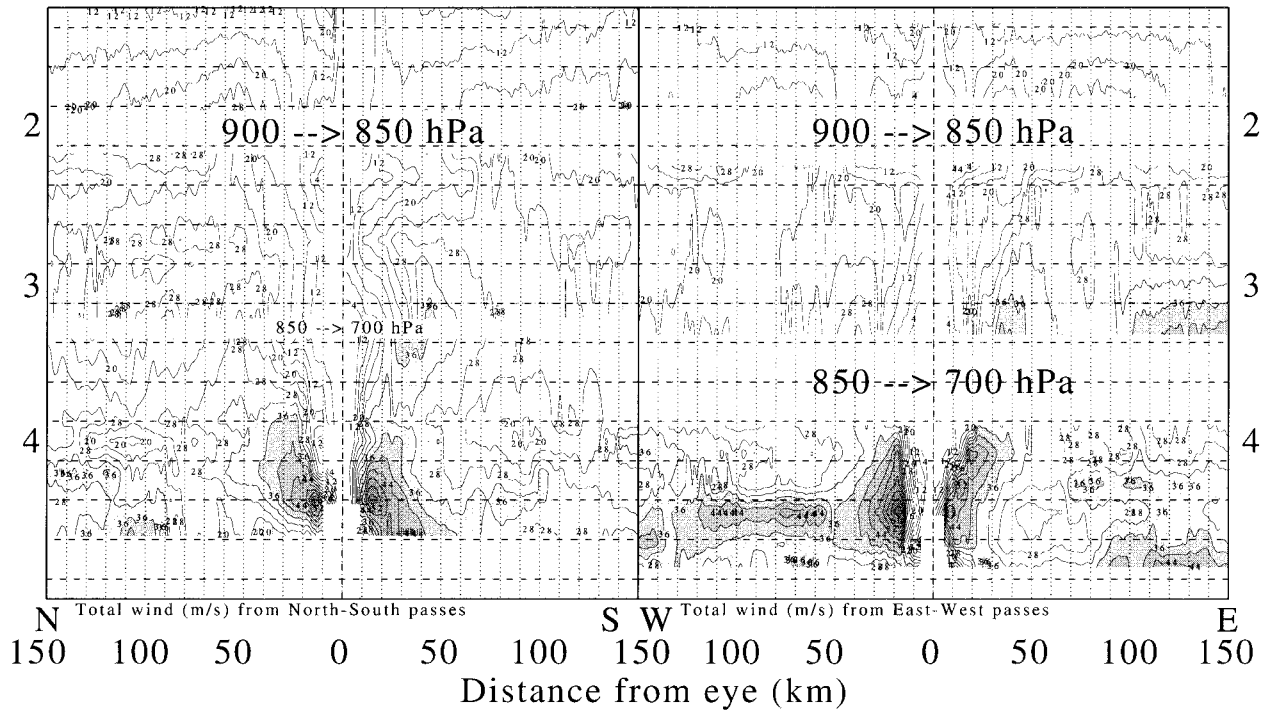


FIG. 12. North-south (left) and east-west (right) time series cross section of reconnaissance aircraft-measured total wind speeds (m s^{-1}) for the period 0600 UTC 1 Oct to 0000 UTC 5 Oct 1995. Each cross section is centered on Opal's eye (vertical dot-dash line) and extends 150 km in either direction (vertical dotted lines every 10 km). The two data gaps on each panel correspond to changes in aircraft and aircraft flight level from the initial 900 hPa to 850 and 700 hPa, respectively. Thin horizontal dashed lines are drawn every 6 h at 0300, 0900, 1500, and 2100 UTC. Numbers on both ordinates denote 0000 UTC on that day.

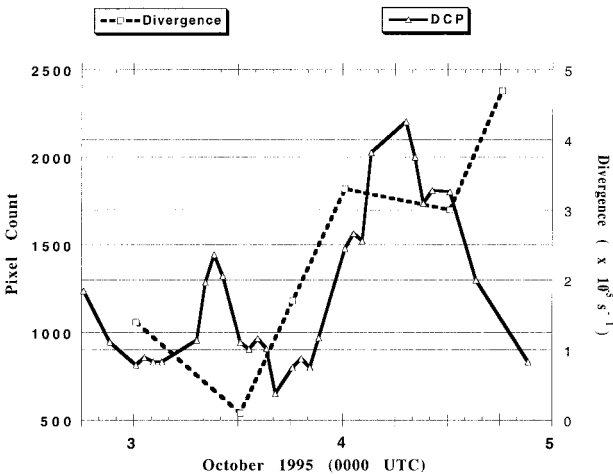


FIG. 13. Time series of GOES 6.7- μm (WV) infrared window (IRW) brightness temperature (BT) difference, defined as the deep convection parameter (DCP, solid line) for the period 1800 UTC 2 Oct–2100 UTC 4 Oct 1995. The DCP is measured by the number of warmer WV pixels (pixel count) relative to collocated IRW pixels. Heavy dashed line denotes 300–200-hPa divergence ($\times 10^{-5} \text{ s}^{-1}$) based on the RF analyses for the period 0000 UTC 3 Oct–1800 UTC 4 Oct 1995. Divergence is computed over a rectangular box poleward of Opal (see text).

The relative DCP minimum between 1200 and 2000 UTC 3 October is interpreted as indirect evidence that the increase in divergence in the upper troposphere is externally generated (trough-jet interaction) and not the result of an increase in the areal extent of deep convection. A more sustained convective burst begins after 2000 UTC 3 October, peaks near 0700 UTC 4 October, and then decreases slightly and plateaus near 0900–1200 UTC 4 October (Fig. 13). The 300–200-hPa divergence pattern changes seem to be clearly associated with the trough in that they vary on synoptic timescales. The divergence increase near the storm is first evident by 1800 UTC 3 October. A divergence increase is not apparent near the storm at 1200 UTC 3 October, despite the initial convective burst near 0900 UTC 3 October. The convective response after 2000 UTC 3 October is consistent with the hypothesis that the rapid intensification phase of Opal may have been triggered by the trough-jet interaction.

d. Oceanic influences

In late summer and early autumn, SSTs over the Gulf of Mexico away from the immediate coastal waters are typically in the 28°–30°C range with small spatial variability. The passage of a tropical storm or hurricane can increase the SST variability through induced mixing

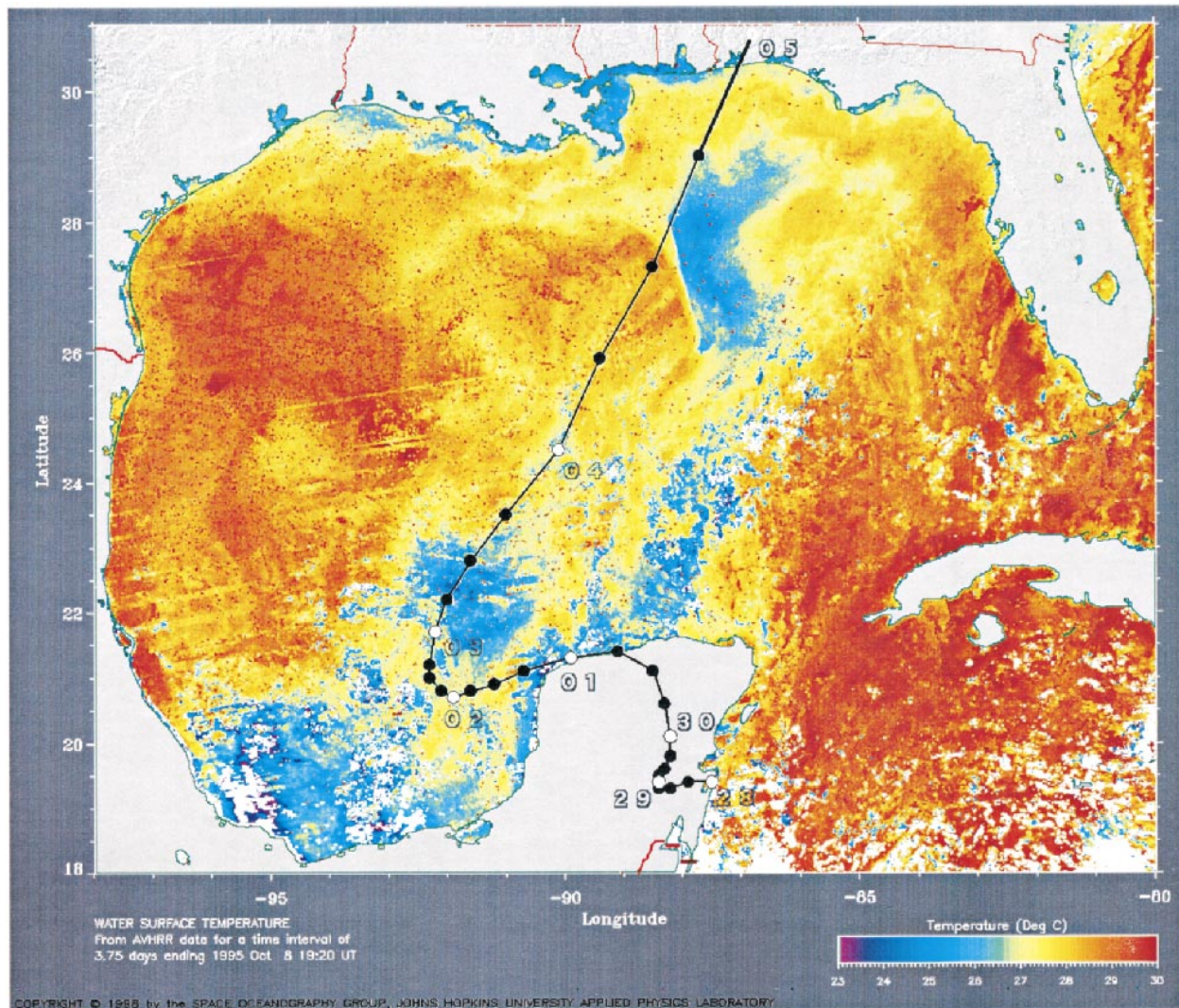


FIG. 14. Gulf of Mexico AVHRR composited sea surface temperature (SST) analysis for the 3.75 days ending 1920 UTC 8 Oct 1995. SST in $^{\circ}\text{C}$ according to the color bar at the lower right. Track of Hurricane Opal is shown from 0000 UTC 28 Sep to 5 Oct 1995 with storm positions indicated every 6 h by the solid circles (white circles denote 0000 UTC position with day adjacent). White splashes indicate where cloud cover was sufficient to preclude a reliable observation. Figure courtesy of the Space Oceanography Group at the Applied Physics Laboratory of the Johns Hopkins University and kindly provided by Joseph Cione of NOAA/AOML/HRD.

where the water is not uniformly warm to a great depth such as would occur in a WCE. An AVHRR image of SSTs over the Gulf for the 3.75-day period ending near 0000 UTC 9 October is shown in Fig. 14 (the image was generated by the Space Oceanography Group at the Johns Hopkins University and kindly made available to the authors by Joseph Cione of NOAA/Atlantic Oceanographic and Meteorological Laboratories (AOML) Hurricane Research Division). On the basis of a comparison to a similar AVHRR image in late September before the Opal crossing, prominent regions of cooling (3° – 5°C) are apparent near and to the west of the Yucatan Peninsula into the Bay of Campeche in the southwest Gulf and over the northeast Gulf of Mexico. The observed SST cooling in the southwest Gulf can prob-

ably be attributed to deep mixing in relatively deep water in association with a prolonged period of above-average winds as Opal was moving very slowly (Fig. 1). The prominent area of SST cooling over the northeast Gulf is over relatively deep water and is concentrated to the right of Opal's track. It is likely that this SST cooling can be attributed to dynamically induced mixing of cooler water from below by the initial bands of strong winds well ahead of the rapidly intensifying storm (Fig. 1). The absence of SST cooling farther to the southeast toward western Cuba is attributed to the presence of the Loop Current and its associated deep layer of warm water. There is also a narrow band of modest ($\sim 2^{\circ}\text{C}$) SST cooling along and just to the right of Opal's track through 0000 UTC 4 October where the

storm accelerated northeastward. Wind-induced mixing is also a likely explanation for this band of cooling.

Relatively little SST cooling is apparent over the north-central Gulf right along Opal's track from ~0300 to 1300 UTC 4 October and in the near-shore waters from southeastern Louisiana eastward to the Florida panhandle. The relative absence of SST cooling from ~0300 to 1300 UTC 4 October can be associated with the passage of Opal across a WCE (Black and Shay 1998; Shay et al. 2000). As shown by Shay et al. (2000), however, a large change in the upper-ocean-layer heat content took place as Opal traversed the WCE. Shay et al. (2000) deduced that this change in heat content in the WCE reservoir had to be associated directly with significant oceanic heat and moisture fluxes into the atmosphere in conjunction with the passage of Opal. Given the relative insensitivity of the observed WCE SST to the passage of Opal, these observations can be reconciled only if the WCE is represented by a deep reservoir of warm water.

A measure of the extent of the reservoir of warm water in the WCE is provided by a TOPEX/Poseidon analysis of SHA for 8–18 September 1995 given in Fig. 15 (analysis kindly provided by Lynn K. Shay of the University of Miami's Rosenstiel School of Marine and Atmospheric Sciences). The WCE is apparent as a quasi-circular region of positive SHA centered near 27.0°N and 89.0°W. In the WCE region the SHA reaches ~50 cm and is indicative of the deep reservoir of warm water where the associated upper-ocean-layer heat content and the potential for appreciable oceanic heat and moisture fluxes in the region to be traversed by Opal is large. Comparison of Figs. 14 and 15 suggests that as Opal crossed the WCE the deep layer of warm water was relatively undisturbed and that use of the AVHRR and TOPEX/Poseidon imagery together may have real-time forecasting applications. Inspection of Fig. 14 shows that Opal's eye reaches the WCE near 0300 UTC 4 October, or ~9 h after the observed increase in areal extent of inner-core deep convection and the onset of rapid intensification and ~3 h after Opal's eyewall tries to close off (recall the SSM/I imagery for 2344 UTC 3 October and 0030 UTC 4 October shown in Fig. 10) as sustained wind speeds increase from 38 to 52 m s⁻¹ (Fig. 2b). Although air parcels on the leading edge of Opal's circulation feel the impact of the WCE and could have reached the eyewall convection prior to the arrival of the eye itself over the WCE, the time lag provides additional indirect evidence that the trough–jet–hurricane interaction initiated the rapid intensification of the storm. The secondary increase in sustained wind speeds from 52 to 68 m s⁻¹ measured between 0600 UTC and 1000 UTC 4 October (Fig. 2b) occurs while Opal's eye is over the WCE.

e. Weakening stage

The weakening stage of Opal begins just before 1200 UTC 4 October (the eye exits the WCE near 1300 UTC

4 October) and continues through the passage of the eye across the coast. Although, presumably, oceanic heat and moisture fluxes are significantly diminished after Opal exits the WCE, the immediate near-shore waters from southeastern Louisiana to the Florida panhandle remain relatively warm (Fig. 14; ~28°C in contrast to 29°–30°C before the storm; not shown). The relative absence of strong and sustained SST cooling in this region might be attributable to 1) the shallow water along the coast being relatively warm from the surface to the bottom before Opal arrived, 2) the homogenization of the shallow warm by mixing with a slightly cooler layer near the bottom superimposed on a small evaporatively cooled component, or 3) the northwestward advection of warm water from the LC along the west coast of Florida in response to the strong southeast winds to the right of Opal's track.

An additional factor in Opal's weakening is likely the observed increase in vertical wind shear that the storm encountered as it makes landfall. The 850–200-hPa shear centered on Opal (position defined by the location of the 850-hPa vorticity maximum) as derived from the ECMWF, NCEP, and RF analyses is shown in Fig. 16 for the period 0000 UTC 1 October to 0000 UTC 5 October along with Opal's minimum central pressure. The shear is computed as the difference between the 350–150-hPa and 950–700-hPa layer-mean winds over a 500-km radius after removal of the storm circulation (following Molinari 1993). As might be expected, the shear values in the coarser resolution NCEP analyses are higher than in the other two analyses. In the ECMWF analysis the 850–200-hPa shear is a minimum (~1 m s⁻¹) at 0000 UTC 4 October when Opal is intensifying rapidly and is still small (~3 m s⁻¹) at 1200 UTC 4 October just after Opal starts to weaken. Subsequently, the shear increases rapidly to 8 m s⁻¹ at 1800 UTC 4 October (not shown) and to ~14 m s⁻¹ by 0000 UTC 5 October as Opal superposes with the larger-scale jet-entrance region (Figs. 8a–f). Agreement between the ECMWF- and RF-derived shear values is generally good with the largest discrepancy occurring at 1200 UTC 4 October when the RF-derived shear has already risen to ~8 m s⁻¹.

f. External influences on hurricane intensity change

Molinari and Vollaro (1989, 1990) applied Eliassen's (1952) BV equation, but in storm-relative coordinates, to help diagnose the interactions of hurricanes with their environment. The solution of Eliassen's BV equation [Eq. (2) in Molinari and Vollaro 1990] yields a radial-vertical circulation that is forced by azimuthally averaged eddy heat and momentum flux convergences. Although a weakness of this approach is that the effects of diabatic heating and friction are not included (these effects are most important within 150 km of the center), useful information on storm–environmental flow interactions can still be assessed by mapping the eddy heat

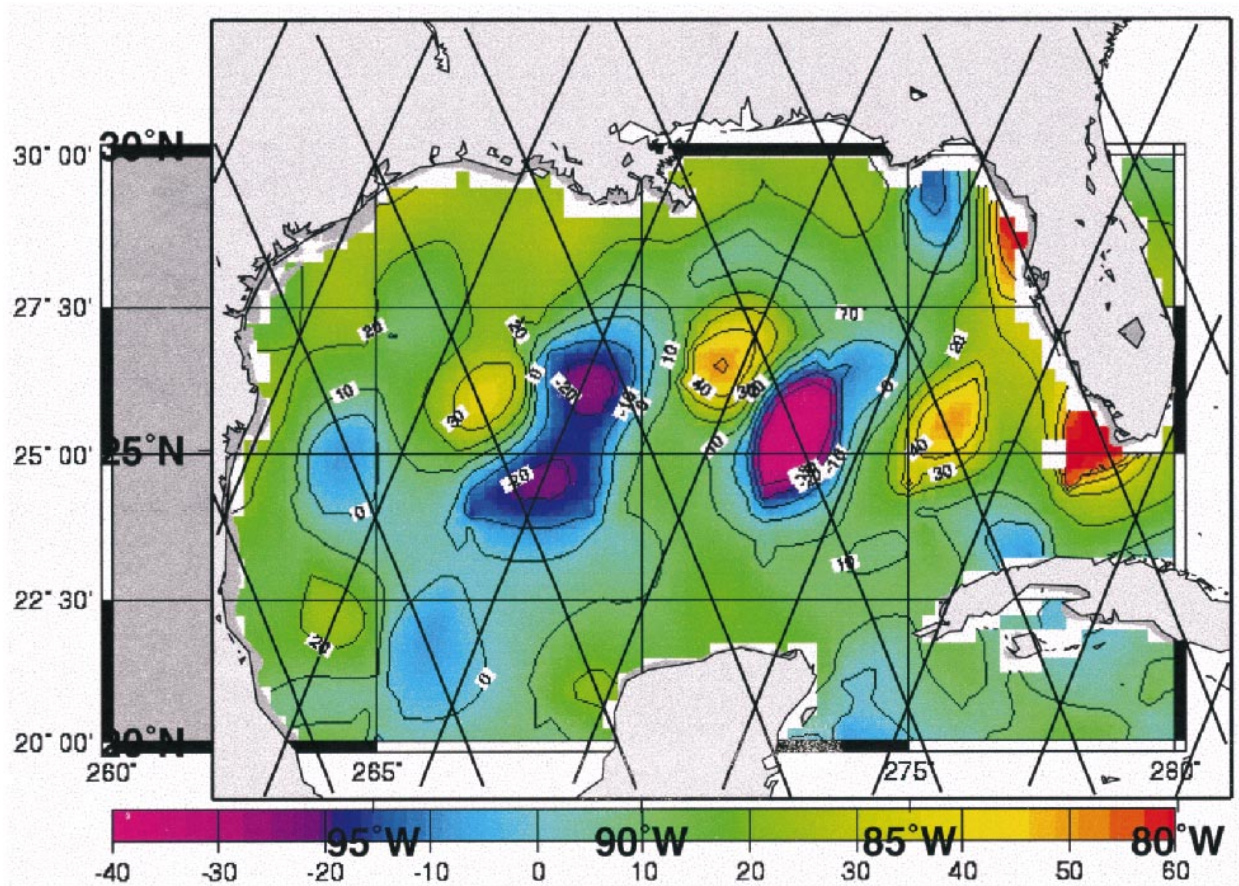


FIG. 15. (a) Pre-Opal TOPEX/Poseidon altimeter-derived sea height anomaly (SHA) for the period 8–18 Sep 1995. SHA values given in cm with warm (cold) colors corresponding to positive (negative) SHA anomalies. Ascending and descending tracks of satellite orbits (~ 315 km apart) shown by crossing solid lines. Width of data footprint ~ 6 km. Figure courtesy of A. J. Mariano and Ryan of the Rosenstiel School of Marine and Atmospheric Sciences (RSMAS) at the University of Miami and kindly provided by Nick Shay of RSMAS.

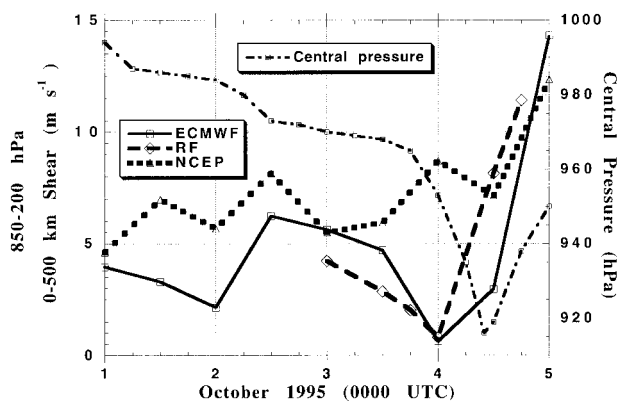


FIG. 16. Time series of computed 850–200-hPa wind shear (m s^{-1}) centered over the 850-hPa grid point with the highest cyclonic vorticity (Opal) for the period 0000 UTC 3–5 Oct 1995. Shear computed from the ECMWF, NCEP, and RF analyses is shown by the solid, dashed, and dashed–dotted lines, respectively. Heavy dashed line denotes aircraft-measured central pressure (hPa) in Opal.

and momentum flux convergences and the BV radial-vertical circulation as demonstrated by Molinari and Vollaro (1990). Here we will restrict ourselves to an analysis of the BV outflow to help assess the importance of Opal–environmental interactions preceding and accompanying the period of rapid intensification. A preliminary analysis revealed that the BV outflow maximized at 200 hPa, a situation found by Molinari and Vollaro (1990) to be true in Hurricane Elena (1985) as well.

Details on the computational procedures can be found in section 4a of Molinari and Vollaro (1990). Briefly, the Eliassen BV equation was solved by successive overrelaxation over a cylindrical volume of radius 2000 km and vertical extent from 1000 to 75 hPa. The grid spacing was 25 km and 25 hPa, respectively, and centered differences were used in all calculations. In addition to the gridded RF analyses, input data consisted of 1.125° (2.5°) ECMWF (NCEP) twice-daily (0000 and 1200 UTC) gridded analyses for all mandatory pressure levels.

Although not shown here, we also computed the 200-

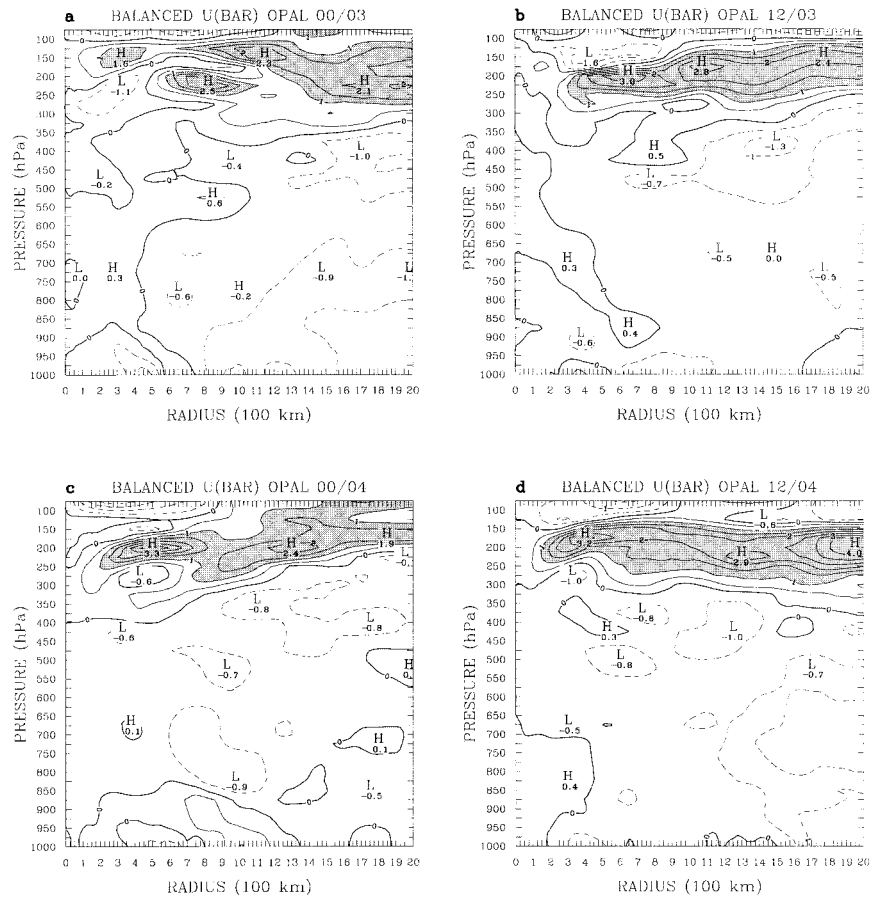


FIG. 17. ECMWF-derived balanced vortex outflow (m s^{-1}) for 0000 and 1200 UTC 3 Oct 1995 (a) and (b), and 0000 and 1200 UTC 4 Oct 1995 (c) and (d). Solid (dashed) contours denote outflow (inflow) with zero contour bold. Outflow values shaded with dark shading beginning at 1 m s^{-1} .

hPa eddy angular momentum flux convergence (EFC) for all three (RF, ECMWF, and NCEP) datasets. In a study of Hurricane Elena (1985), Molinari and Vollaro (1989, 1990) found that a hurricane–trough interaction could be associated with a progressive inward shift of positive values of EFC (forcing for a cyclonic circulation) from beyond 1000 km to within 500 km of the storm’s core. Positive values of EFC were computed (with large variability) from all three datasets inward of 500 km near 0000 UTC 4 October. Because of the large computed EFC variability within 500 km of the storm’s core where Molinari and Vollaro (1989) showed typical error rates of $>50\%$, we are reluctant to draw firm conclusions from the EFC results. We will show, however, the BV outflow solutions, given that the calculated outflow is very robust because it represents a reduction of the forcing.

The azimuthally averaged BV outflow (ECMWF analyses only) is shown in Fig. 17 as a function of storm radius and pressure for the period 0000 UTC 3 October through 1200 UTC 4 October. The BV outflow ($\sim 2\text{--}3 \text{ m s}^{-1}$) maximizes near 200 hPa throughout with the

suggestion of inner and outer maxima. (For perspective purposes note that a typical mean radial velocity in a storm outflow layer is $5\text{--}10 \text{ m s}^{-1}$. Our calculation is dry; thus 3 m s^{-1} is substantial.) The broad BV outflow becomes well organized by 1200 UTC 3 October. It also exhibits a tendency to lower from 150 hPa to 200 hPa by 1200 UTC 4 October as Opal approaches the mid-latitude trough and associated lower tropopause. The inner BV outflow maximum, initially situated near 800 km at 1200 UTC 3 October, becomes more concentrated as it shifts inward to near 500 and 400 km at 0000 and 1200 UTC 4 October, respectively. This feature can probably be associated with an inner band for cyclonic EFC forcing (not shown). The outer BV outflow maximum stays more diffuse and can be associated with an outer band for cyclonic EFC forcing (not shown).

Displayed in Fig. 18 is the 200-hPa BV outflow averaged over 0–600 km and calculated from both the ECMWF and NCEP analyses for the period 0000 UTC 1 October–0000 UTC 5 October. At 0000 UTC 2 October as Opal starts to recurve poleward (Fig. 1) a modest intensification is about to begin as measured by a

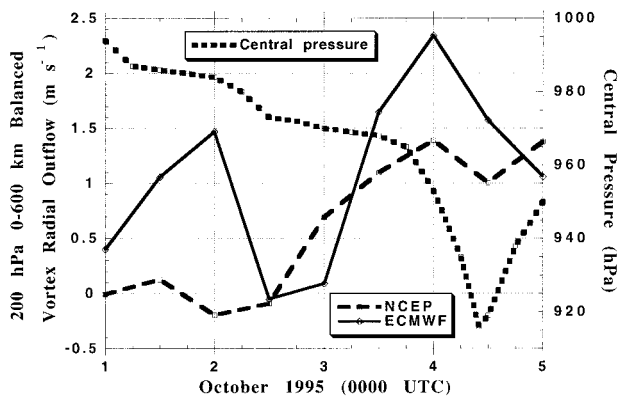


FIG. 18. The 200-hPa azimuthally averaged balanced vortex outflow (m s^{-1}) for the period 0000 UTC 1–5 Oct 1995 for the ECMWF (NCEP) analyses as shown by the solid (dashed) curve. Central pressure (hPa) in Opal is shown dotted.

12-hPa central pressure decrease in the next 12 h. The ECMWF-derived BV outflow exhibits its first maximum ($\sim 1.5 \text{ m s}^{-1}$) at 0000 UTC 2 October, suggestive of a possible environmental flow–storm interaction. This first BV outflow maximum is absent from the coarser resolution NCEP-derived calculation. Although an investigation of the modest intensification (central pressure decrease of $\sim 20 \text{ hPa}$; Fig. 2a) of Opal in the 18-h period ending 1200 UTC 2 October is beyond the scope of this paper, inspection of the ECMWF analyses (not shown) reveals a slight strengthening of the westerlies over the northwest Gulf of Mexico and a weakening (strengthening) of the northerly (southwesterly) flow to the west (east) of Opal. These subtle flow changes are consistent with the onset of a slow turn of the storm to the northeast (Fig. 1). The second, and largest, BV outflow peak computed from the ECMWF analyses (1.5 and 2.3 m s^{-1} , respectively, at 1200 UTC 3 October and 0000 UTC 4 October) coincides with the rapid intensification phase of Opal. The BV outflow computed from the NCEP analyses exhibits a broader and flatter maximum from 1200 UTC 3 October to 0000 UTC 5 October with no suggestion for a weakening by 1200 UTC 4 October as is computed from the ECMWF analyses. These findings suggest that the rapid intensification phase of Opal is likely influenced by environmental flow–storm interaction processes. The environmental flow–storm interaction signature is sharper and better defined in calculations made from the higher-resolution ECMWF analyses.

Shown in Figs. 19 and 20 are the ECMWF and NCEP 300–200-hPa layer-averaged streamlines, isotachs, absolute vorticity, divergence, and divergence change for 1200 UTC and 1800 UTC 3 October and 0000 UTC 4 October. These figures should be compared with the corresponding RF analyses presented in Figs. 6d–f, 7a–f and the high density WV winds plotted in Fig. 4b and Figs. 5a,b. Important differences are readily apparent between the higher (lower) resolution ECMWF (NCEP)

analyses. The ECMWF analyses replicate the observed southerly and south-southeasterly outflow poleward of Opal to the south of Louisiana (cf. Figs. 19a–c with Figs. 4b and 5a,b) more accurately than do the NCEP analyses (Figs. 20a–c) at all three times. Likewise, the ECMWF analyses show the development of a secondary 300–200-hPa layer-averaged divergence maximum just poleward of Opal by 1800 UTC 3 October, a feature that persists at 0000 UTC 4 October (Figs. 19e–f). This ECMWF-derived divergence pattern is consistent with the RF-derived divergence analysis presented in Figs. 7b and 7e. The coarser-resolution NCEP analyses do not capture this divergence signal (Figs. 20d–f).

Similarly, the NCEP analyses are unable to maintain a region of lighter winds ($< 10 \text{ m s}^{-1}$) near the center of Opal as compared to the ECMWF and RF analyses (cf. Figs. 19a–c with Figs. 20a–c and Figs. 6d, 7a, 7d). The stronger 850–200-hPa shear within 500 km of Opal computed from the NCEP analyses (Fig. 16) is also consistent with this interpretation. Another subtle flow signature difference can be found by comparing the structure of the equatorward jet-entrance region near coastal Louisiana and associated absolute vorticity patterns in all three analyses. In the RF and ECMWF analyses there is an area of 300–200-hPa layer-averaged wind speeds under 5 m s^{-1} to the northwest of Opal for the period 1200 UTC 3 October to 0000 UTC 4 October. The juxtaposition of this light wind region near Opal (and associated weak shear) ensures that the equatorward jet-entrance region near the Louisiana coast is effectively shifted toward Opal along the westward flank of the strengthening outflow region (cf. Figs. 19a–c and Figs. 6f, 7c, and 7f). This shift is also manifest in the approach of the vorticity in the jet tail toward the Opal vorticity maximum in the 12 h ending 0000 UTC that is seen in the RF and ECMWF analyses. Similarly, the “shift” of the equatorward jet-entrance region toward Opal is consistent with the increase in divergence just poleward of Opal in both the RF and ECMWF analyses. It is also consistent with the increase in deep ascent within 600 km of Opal (not shown) that must be associated with the computed maximum 200-hPa BV outflow at 0000 UTC 4 October from the ECMWF analyses (Fig. 18). The coarser-resolution NCEP analyses smear out the jet-entrance region isotach and associated divergence and vorticity structure.

5. Concluding discussion

The critical operational problem posed by Hurricane Opal was the unpredicted (by models and forecasters alike) explosive intensification of the storm over the Gulf of Mexico. Our study was motivated by the observation that environmental influences apparently played a role in the unpredicted intensification. A high-density, GOES-8 WV wind dataset was used to construct a series of sequential high-resolution upper-tropospheric wind analyses over the Gulf. Diagnostic analyses of

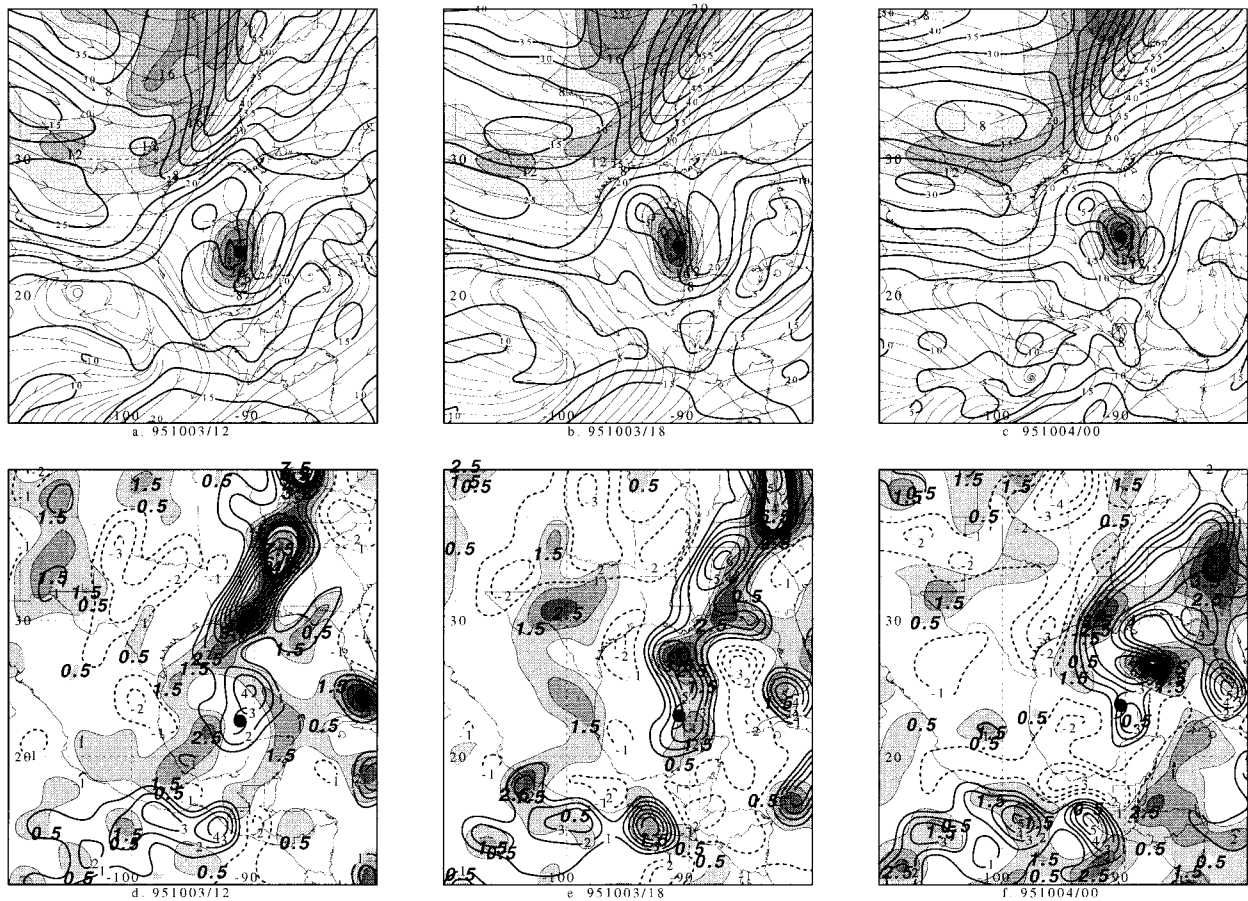


FIG. 19. ECMWF analyses of (a) streamlines (thin solid), isotachs (heavy solid, every 50 m s^{-1}), and absolute vorticity (shaded beginning every $8 \times 10^{-5} \text{ s}^{-1}$ according to the scale) for 1200 UTC 3 Oct 1995; (b) and (c) as in (a) except for 1800 UTC 3 Oct 1995 and 0000 UTC 4 Oct 1995, respectively. (d) Divergence every $1 \times 10^{-5} \text{ s}^{-1}$ with positive (negative) values drawn solid (dashed) and zero contour omitted; 6-h divergence change (positive values only) is drawn shaded every $1.0 \times 10^{-5} \text{ s}^{-1}$ beginning at $0.5 \times 10^{-5} \text{ s}^{-1}$ according to the scale for 1200 UTC 3 Oct 1995; (e) and (f) as in (d) except for 1800 UTC 3 Oct 1995 and 0000 UTC 4 Oct 1995, respectively. Location of Opal is denoted by the conventional hurricane symbol in all panels.

300–200-hPa layer-averaged divergence and vorticity constructed from these wind analyses indicated a significant increase in upper-tropospheric divergence over and poleward of Opal just prior to and during the onset of the unpredicted rapid intensification as Opal interacted with a trough tail/jet-entrance region. During this interaction and prior to the arrival of Opal's eye over the WCE a sustained wind speed increase from 38 to 52 m s^{-1} was measured.

To help put the Opal development into perspective, a calculation of the maximum potential intensity (MPI) hurricane wind speed was made after Emanuel (1995). The MPI represents a theoretical upper bound on tropical cyclone intensity based upon available thermodynamic profiles and SSTs. The daily NCEP reanalysis fields (Kalnay et al. 1996) and the weekly SST analyses made available by the National Environmental Satellite Data Information Service have been used to construct the MPI time series shown in Fig. 21. Most importantly,

Opal has the potential for significant development (i.e., it is far from its MPI) prior to and at the onset of rapid intensification (1200 UTC 3 October–0000 UTC 4 October) as the trough–jet–hurricane interaction begins. Accordingly, we hypothesize that the effectiveness of hurricane–trough interactions on intensification will be highly dependent upon how far the storm is from its MPI during the period of interaction.

Based upon the ECMWF datasets (and supported by the RF analyses), when Opal is far below its MPI there is an initial rapid increase in BV outflow at 200 hPa at 1200 UTC 3 October (Fig. 18) that peaks at 0000 UTC 4 October at a time when the 850–200-hPa shear is near 1 m s^{-1} (Fig. 16). Because Opal is far below its MPI at the onset of rapid intensification the trough–jet–hurricane interaction, as reflected in the BV outflow results, must play an important role in the initiation of the rapid intensification. A further boost to rapid intensification begins after 0300 UTC 4 October as Opal's eye crosses

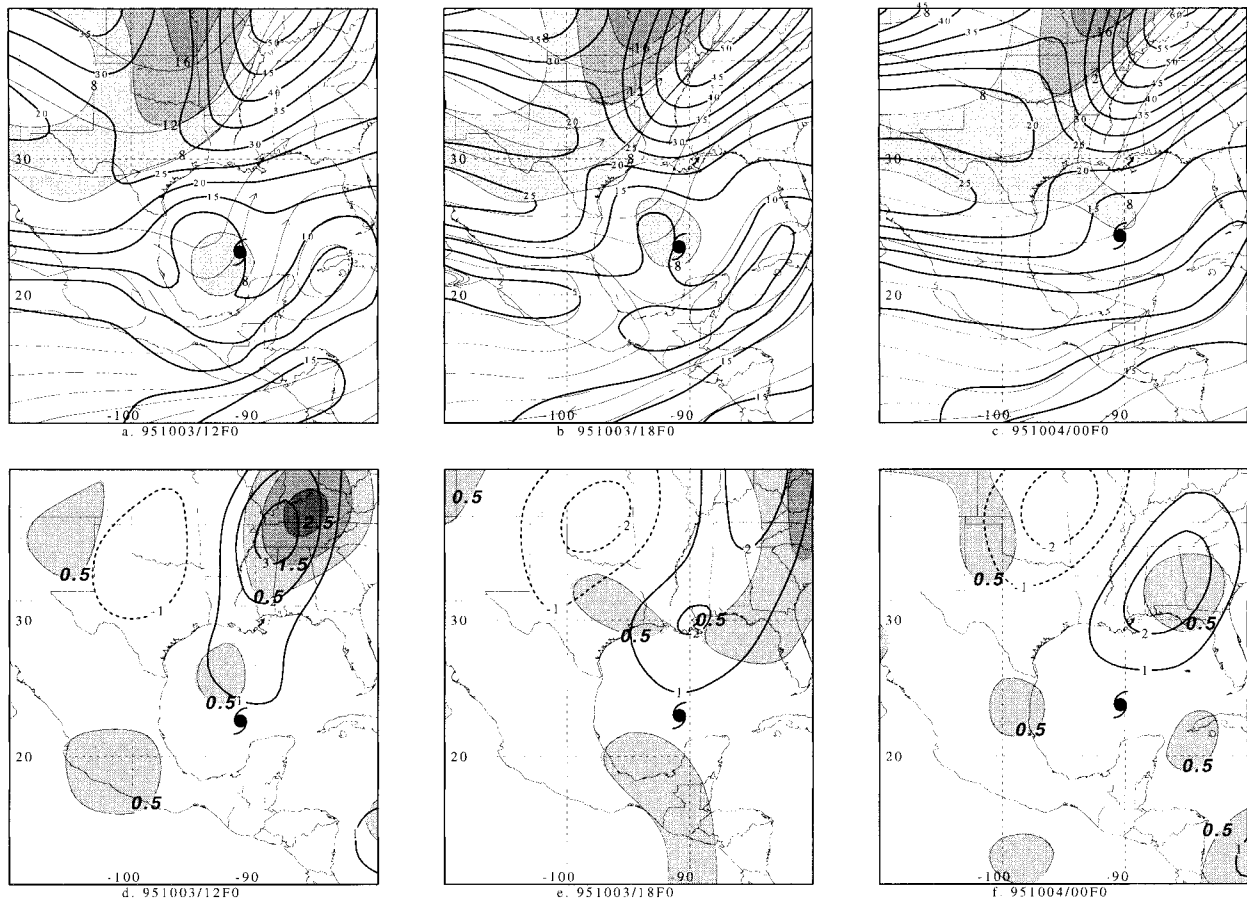


FIG. 20. As in Fig. 19 except based on the NCEP analyses.

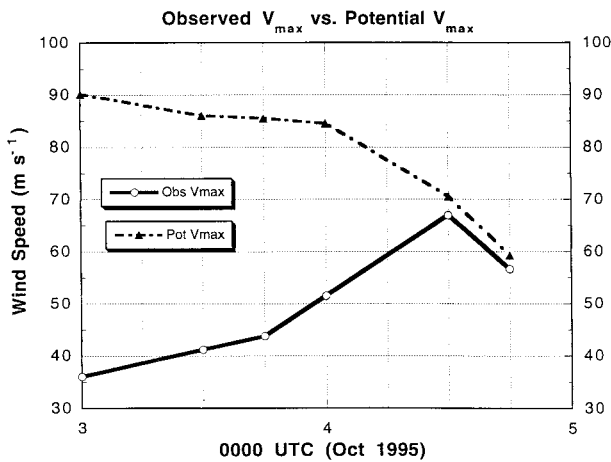


FIG. 21. Times series of the theoretical maximum potential intensity (MPI) wind speed (dash-dot line with solid triangles, $m s^{-1}$) and observed maximum wind speed (solid line with open circles, $m s^{-1}$) for Opal for the period 0000 UTC 3–5 Oct 1995. Vertical dotted lines every 6 h. MPI is computed according to Emanuel (1995).

the WCE and is seen in the sustained wind speed increase from 52 to $68 m s^{-1}$ between 0600 UTC and 1000 UTC 4 October (Fig. 2b). By 1200 UTC 4 October Opal is already weakening as the storm reaches (or even exceeds its MPI), the 850–200-hPa shear starts to increase rapidly, its eye is about to exit the WCE, the 200-hPa BV outflow begins to decrease, and a possible eyewall replacement cycle (internal dynamical process) is in progress. The approaching synoptic-scale trough is too big and has too much shear to impact Opal (other than negatively) with the storm near its MPI. When a storm is near its MPI even a “perfect” trough with low shear will have little impact on further intensification.

Our interpretation of this result is that the upper-tropospheric divergence associated with the trough–jet–hurricane interaction that begins near 1500 UTC 3 October helps to trigger the areal expansion of deep eyewall convection that begins slowly near 1700 UTC 3 October, intensifies after 2100 UTC 3 October, and then briefly peaks near 0100 UTC 4 October with the completion of the first stage of rapid intensification (Figs. 2a and 13). We suggest that the divergence increase is not a result of deep convection but is instead a result of the trough–jet–storm interaction. In our view this

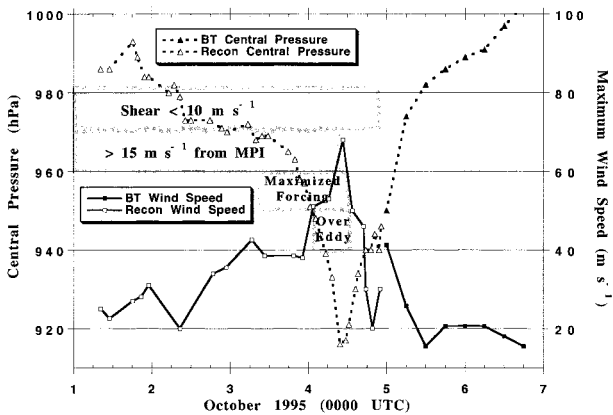


FIG. 22. Opal central pressure (hPa, heavy solid line) and maximum eyewall wind speed (m s^{-1} , heavy dotted line) for the period 0000 UTC 1–7 Oct 1995. Solid (open) squares and triangles denote aircraft reconnaissance measured (NHC best track) storm central pressure and maximum flight level winds (see Fig. 12 for flight levels). Shaded horizontal bars denote (from top to bottom) when the 850–200-hPa shear averaged over 0–500 km and centered on the 850-hPa vorticity maximum is $< 10 \text{ m s}^{-1}$, the observed maximum winds in Opal are more than 15 m s^{-1} below the MPI, the 0–600-km azimuthally averaged balanced vortex outflow in the ECMWF analyses exceeds 1.5 m s^{-1} , and Opal's eye is over the oceanic warm-core eddy.

interaction, and resulting increase in deep mesoscale ascent, is what triggers the observed increase in convection and the initial onset of rapid intensification. Rapid intensification resumes (second stage) as Opal reaches the WCE near 0300 UTC 4 October (note the second surge in the sustained winds as the DCP increases further near 0600 UTC 4 October as shown in Figs. 2a, 13) as the storm is able to feed off of large oceanic heat and moisture fluxes from the deep layer of warm water in the WCE (Shay et al. 2000; Hong et al. 2000) in an environment still favorable for intensification via a trough-jet-storm interaction (Figs. 17, 18). Opal, close to its MPI at 1200 UTC 4 October, cannot intensify any further as it leaves the WCE region at ~ 1300 UTC 4 October (Fig. 14) and is absorbed into the jet-entrance region of the larger-scale trough where it encounters increasing 850–200-hPa shear (Fig. 16). A schematic summary of the physical processes believed to be important to the intensification of Opal is shown in Fig. 22.

It is our view that the question of what is meant by a hurricane–trough interaction is inextricably linked with the question of how a synoptic-scale trough interacts with a mesoscale hurricane. This raises the question of what is a “good” trough and what is a “bad” trough, where good and bad refer to a positive and negative impact on development, respectively. Studies of other storms such as Diana (Bosart and Bartlo 1991), David (e.g., Bosart and Lackmann 1995), and Elena (Velden 1987; Molinari et al. 1995, 1998) also suggest that a good trough should have a lateral scale comparable to the scale of the tropical storm. Given that forcing for ascent by differential vorticity advection at the level of

QG theory is inversely proportional to the square of the length scale, smaller-scale troughs can be associated with vigorous near-mesoscale ascent, especially if the static stability is relatively small. The results from this paper suggest that good and bad troughs can be further stratified on the basis of how far the storm is from its MPI at the time of the hurricane–trough interaction.

In case studies by Molinari et al. (1995), Bosart and Bartlo (1991), and Bosart and Lackmann (1995), and in the idealized study of Montgomery and Farrell (1993), a PV anomaly aloft approaches but never over-spreads the developing storm. Although there is positive PV advection over each developing storm, a necessary condition to force ascent, the PV anomaly is gradually isolated from the main PV reservoir and then mostly eradicated in response to diabatically driven ridging aloft over the storm. In effect, synoptic-scale wave breaking is induced, in part, by the hurricane–outflow anticyclone (Molinari et al. 1995). This synoptic-scale wave breaking is manifest as anticyclogenesis aloft and the isolation (fracture) of the original PV anomaly from the main PV reservoir.

Our assertion is that a good trough should be typified by a fractured PV anomaly that is comparable in scale to the size of the tropical storm and much smaller than the scale of the original trough from which it fractured (Molinari et al. 1998). (Note that preexisting cold lows or isolated PV anomalies in the tropical upper troposphere may also have the correct scale characteristics.) Mesoscale ascent associated with the trough/PV anomaly likely helps to organize deep convection, thereby resulting in an upscale development as individual thunderstorms form into clusters. In effect, the trough is “downsized” so that it is more comparable to the scale of the “upsized” area of organized deep convection. A “downsized” trough would also likely have less vertical shear and would therefore be more favorable for tropical storm development or intensification.

Opal is a more complex case than the examples cited earlier because the storm went through several intensification cycles beginning with its initial intensification to tropical storm strength while over land (Fig. 3 and Bracken and Bosart 1998). As Opal accelerated northeastward across the Gulf it approached a trough tail/jet-entrance region located from coastal southern Texas to southwestern Louisiana. Increased ridging and anticyclonic curvature aloft in the Opal outflow subsequent to 1200 UTC 3 October helped to block the eastward movement of the equatorward end of the coastal Texas trough and could be associated with a persistent deformation zone over the northwest Gulf of Mexico. This deformation zone was marked on its eastern end by increasing outflow poleward of Opal as winds aloft backed to southerly and south-southeasterly. The outflow pattern was likely a reflection of diabatic warming associated with deep convection well removed from the storm center (Figs. 10, 11), analogous to the flow configuration presented by Bosart and Carr (1978; their Fig.

13) as conducive to heavy rains well in advance of a tropical storm. This interpretation is consistent with the expansion of a mass of deep cloudiness and convective precipitation poleward of Opal after 1200 UTC 3 October seen in the WV and SSM/I imagery (Figs. 9, 10).

A critical unresolved issue is how our postulated trough–jet–hurricane dynamical interaction actually fosters communication with the inner-core storm dynamics. In the case of Hurricane Elena (1985) Molinari and Vollaro (1990) showed that the approach of a midlatitude trough produced an area of positive (cyclonic) EFC that progressed radially inward and could be associated with a band of enhanced ascent. The associated inward-propagating BV outflow circulation was assumed to have excited an internal instability in the inner convection area that contributed to the intensification of the storm. A similar analysis here suggests that the 200-hPa BV outflow circulation associated with the synoptic-scale trough was too far removed from Opal (>1000 km) to have much of a dynamical impact and that at the time this trough was closest to Opal the storm was near its MPI and unable to respond to the external stimulation. The azimuthally averaged 200-hPa BV outflow results, however, suggested that a subsynoptic-scale trough–jet–hurricane interaction contributed to the rapid intensification phase of Opal (Fig. 18). External–internal dynamical interactions may also perhaps occur through convectively induced low-level PV maxima as discussed theoretically by Montgomery and Kallenbach (1997) and Montgomery and Enogonio (1998) (section 4c) or by means of angular momentum exchanges modified by convection along storm inflow–outflow channels (Krishnamurti et al. 1998).

A critical forecast issue is whether there are any identifiable parameters that can be used to determine whether an upper-tropospheric trough will weaken or strengthen a tropical cyclone. Although every case will be different, the scale-matching concept discussed above appears to be fundamental to the forecast. Particular attention needs to be paid to troughs that show evidence of fracturing from the midlatitude westerlies. Fractured troughs that exhibit the potential to be juxtaposed near preexisting disturbances or storms in the easterlies, or even inactive other nearby upper-level cold-core cutoff cyclones, must be scrutinized especially carefully by forecasters. This scrutiny is warranted because such a flow arrangement is favorable for genesis and/or intensification via lateral and vertical PV anomaly interactions. The configuration and scale of troughs relative to the overall upper-level flow and existing low-level disturbances and their evolution is critical to the forecast process. Dynamically, some shear is required in order that advective processes such as differential vorticity advection and the Laplacian of thermal advection can force subsynoptic-scale ascent and help organize deep convection. Positive PV advection associated with a smaller-scale PV anomaly can contribute to storm development by forcing subsynoptic-scale ascent over part of

the storm. In response, asymmetric deep convection can erupt while the associated diabatic heating can lead to the creation of a favorable anticyclonic outflow environment and reduced shear over the storm.

A critical scientific (and forecast) issue is how the storm inner-core dynamical processes are signaled and activated by a PV anomaly interaction. Even though the 200-hPa azimuthally averaged BV outflow calculations show good evidence for a hurricane–trough–jet interaction at the onset of rapid deepening, this calculation does not include the effects of diabatic heating. The SSM/I imagery clearly shows an eruption of deep convection in the eyewall near 0000 UTC 4 October after the first stage of rapid intensification had commenced (Fig. 10). The diabatic heating associated with the deep convection could be contributing to a secondary circulation that produces ascent in the eyewall and descent within the eye and can lead to a decrease in storm central pressure and an increase in eyewall wind speeds. Further observational, numerical, and theoretical studies will be needed to address these issues.

Last, the question arises as to why the ECMWF (and to lesser extent the NCEP) analyses yield BV outflow solutions supportive of jet–trough–hurricane interactions whereas the model forecasts based on these analyses were woeful. Our interpretation of this apparent conundrum is that although the ECMWF analyses capture the interaction between Opal and its environment well, it does not necessarily follow that numerical forecasts based on these analyses can simulate the response to that interaction successfully. A much higher resolution model with better physics is needed to address this problem. As far as the ECMWF model (1995 version) was concerned Opal did not possess an eye. It is our view that a successful prediction of intensity change will require a simulation of deep convection in the eyewall and adequate resolution of the eye and inner storm structure. It is also our view that the successful prediction of intensity change will require enhanced mesoscale observations within the storm region and its environment. We temper these views with the knowledge, however, that for Opal that hurricane models initialized with larger-scale fields still did not predict the observed hurricane intensity change properly and that reasons for this failure need to be addressed.

The high spatial and temporal resolution afforded by the *GOES-8* WV winds proved to be very helpful in revealing many “details” of the trough–jet–hurricane interaction (e.g., the outflow poleward of Opal) that a forecaster would consider important to the hurricane intensity change problem. Likewise, the storm-centered 0–500-km 850–200-hPa shear based upon the *GOES-8* WV winds showed reduced shear values compared to the ECMWF analyses at 1200 UTC–1800 UTC 3 October as the initial trough–jet–hurricane interaction began and, equally important from an operational perspective, the *GOES-8* WV winds revealed substantially increased shear by 1200 UTC 4 October relative to the

ECMWF analyses at which time Opal had ceased intensifying and had begun weakening (Fig. 16). At issue is how to obtain the benefits of the high spatial and temporal resolution GOES-8 WV winds in a modern four-dimensional data analysis and initialization scheme, given that the uncertainty of the level assignment of the wind vectors can exceed the vertical resolution in the operational prediction model.

Acknowledgments. We gratefully acknowledge Steve Wanzong of UW-CIMSS and David Vollaro of SUNY/Albany for help with the calculations. Jeff Hawkins of the Naval Research Laboratories in Monterey, California, is thanked for providing us with high quality SSM/I imagery. Joe Cione of NOAA/AOML/HRD provided the AVHRR imagery for Opal. Nick Shay of the Rosenstiel School of Marine and Atmospheric Sciences at the University of Miami is thanked for stimulating discussions on the importance of the oceanographic contribution to the rapid intensification of Opal and for providing us TOPEX/Poseidon analyses. The final manuscript was significantly improved thanks to the critical comments of Chris Davis, Mark DeMaria, and one other anonymous referee. This research was supported by NSF Grant ATM-9612485, ONR Grant N00014-94-1-0289, and NOAA Grant 50WCNE-306075.

REFERENCES

- Bender, M. A., I. Ginis, and Y. Kurihara, 1993: Numerical simulations of tropical cyclone-ocean interaction with a high resolution coupled model. *J. Geophys. Res.*, **98**, 23 245–23 263.
- Black, P. G., 1977: Some aspects of tropical storm structure revealed by hand held camera photographs from space. *Skylab Explores the Earth*, NASA, 417–461.
- , 1983: Tropical storm structure revealed by stereoscopic photographs from Skylab. *Adv. Space Res.*, **2**, 115–124.
- , and L. K. Shay, 1998: Observations of tropical cyclone intensity change due to air-sea interaction processes. Preprints, *Symp. on Tropical Cyclone Intensity Change*, Phoenix, AZ, Amer. Meteor. Soc., 161–168.
- Bosart, L. F., and F. H. Carr, 1978: A case study of excessive rainfall centered around Wellsville, New York, 20–21 June 1972. *Mon. Wea. Rev.*, **106**, 348–362.
- , and J. A. Bartlo, 1991: Tropical storm formation in a baroclinic environment. *Mon. Wea. Rev.*, **119**, 1979–2013.
- , and G. M. Lackmann, 1995: Postlandfall tropical cyclone re-intensification in a weakly baroclinic environment: A case study of Hurricane David (September 1979). *Mon. Wea. Rev.*, **123**, 3268–3291.
- Bracken, W. E., and L. F. Bosart, 1998: Multiple development aspects of Hurricane Opal (1995). Preprints, *Symp. on Tropical Cyclone Intensity Change*, Phoenix, AZ, Amer. Meteor. Soc., 99–104.
- Briegel, L. M., and W. M. Frank, 1997: Large-scale influences on tropical cyclogenesis in the western North Pacific. *Mon. Wea. Rev.*, **125**, 1397–1413.
- Burpee, R. W., J. L. Franklin, S. J. Lord, R. E. Tuleya, and S. D. Aberson, 1996: The impact of Omega dropwindsondes on operational hurricane track forecast models. *Bull. Amer. Meteor. Soc.*, **77**, 925–933.
- Challa, M., and R. L. Pfeiffer, 1990: Formation of Atlantic hurricanes from cloud clusters and depressions. *J. Atmos. Sci.*, **47**, 909–927.
- , —, Q. Zhao, and S. W. Chang, 1998: Can eddy fluxes serve as a catalyst for hurricane and typhoon formation? *J. Atmos. Sci.*, **55**, 2201–2219.
- Colón, J. A., and W. R. Nightingale, 1963: Development of tropical cyclones in relation to circulation patterns at the 200 millibar level. *Mon. Wea. Rev.*, **91**, 329–336.
- Dean, D. B., and L. F. Bosart, 1996: Northern Hemisphere 500 hPa trough merger and fracture: A climatology and case study. *Mon. Wea. Rev.*, **124**, 2644–2671.
- DeMaria, M., 1996: The effect of vertical shear on tropical cyclone intensity change. *J. Atmos. Sci.*, **53**, 2076–2087.
- , and J. Kaplan, 1997: An operational evaluation of a statistical hurricane prediction scheme (SHIPS). Preprints, *22d Conf. on Hurricanes and Tropical Meteorology*, Fort Collins, CO, Amer. Meteor. Soc., 280–281.
- , and M. M. Huber, 1998: The effect of vertical shear on tropical cyclone intensity change: An historical perspective. Preprints, *Symp. on Tropical Cyclone Intensity Change*, Phoenix, AZ, Amer. Meteor. Soc., 22–29.
- Dickinson, M. J., L. F. Bosart, W. E. Bracken, G. J. Hakim, D. M. Schultz, M. A. Bedrick, and K. R. Tyle, 1997: The March 1993 Superstorm cyclogenesis: Incipient phase synoptic- and convective-scale flow interaction and model performance. *Mon. Wea. Rev.*, **125**, 3041–3072.
- Eliassen, A., 1952: Slow thermally or frictionally controlled meridional circulation in a circular vortex. *Astrophys. Norv.*, **5**, 19–60.
- Elsberry, R. L., and R. A. Jeffries, 1996: Vertical wind shear influences on tropical cyclone formation and intensification during TCM-92 and TCM-93. *Mon. Wea. Rev.*, **124**, 1374–1387.
- , G. Holland, H. Gerrish, M. DeMaria, C. Guard, and K. A. Emanuel, 1992: Is there any hope of tropical cyclone intensity prediction?—A panel discussion. *Bull. Amer. Meteor. Soc.*, **73**, 264–275.
- Emanuel, K. A., 1986: An air-sea interaction theory for tropical cyclones. Part I: Steady-state maintenance. *J. Atmos. Sci.*, **43**, 585–604.
- , 1991: The theory of hurricanes. *Annu. Rev. Fluid Mech.*, **23**, 179–196.
- , 1995: Sensitivity of tropical cyclones to surface exchange coefficients and a revised steady-state model incorporating eye dynamics. *J. Atmos. Sci.*, **52**, 3969–3976.
- , 1998: Theoretical and numerical modeling inferences on the feedback of ocean dynamics on hurricane intensity. Preprints, *Symp. on Tropical Cyclone Intensity Change*, Phoenix, AZ, Amer. Meteor. Soc., 154–160.
- Erickson, C. O., 1967: Some aspects of the development of Hurricane Dorothy (1966). *Mon. Wea. Rev.*, **95**, 121–130.
- Frank, W. M., 1977: Convective fluxes in tropical cyclones. *J. Atmos. Sci.*, **34**, 1554–1568.
- Goni, G. J., S. L. Garzoli, A. Roubicek, D. B. Olsen, and O. B. Brown, 1997: Agulhas ring dynamics from TOPEX/Poseidon satellite altimeter data. *J. Mar. Res.*, **55**, 861–883.
- Hawkins, J. D., K. Richardson, G. Sandlin, G. Poe, C. Velden, and D. May, 1995: Tropical cyclone intensity and structure estimates via satellite multi-sensor techniques. Preprints, *21st Conf. on Hurricanes and Tropical Meteorology*, Miami, FL, Amer. Meteor. Soc., 631–633.
- , D. A. May, and M. J. Helveston, 1998: Satellite tools for monitoring tropical cyclone intensity change. Preprints, *Symp. on Tropical Cyclone Intensity Change*, Phoenix, AZ, Amer. Meteor. Soc., 51–55.
- Hayden, C. M., and R. J. Purser, 1988: Three-dimensional recursive filter objective analysis of meteorological fields. Preprints, *Eighth Conf. on Numerical Weather Prediction*, Baltimore, MD, Amer. Meteor. Soc., 185–190.
- , and —, 1995: Recursive filter objective analysis of meteorological fields: Applications to NESDIS operational processing. *J. Appl. Meteor.*, **34**, 3–15.
- Holland, G. J., 1997: The maximum potential intensity of tropical cyclones. *J. Atmos. Sci.*, **54**, 2519–2541.

- , and Y. Wang, 1998: On the relative roles of lateral interactions and thermodynamics in tropical cyclone intensification. Preprints, *Symp. on Tropical Cyclone Intensity Change*, Phoenix, AZ, Amer. Meteor. Soc., 171–175.
- Hong, X., S. W. Chang, S. Raman, L. K. Shay, and R. Hodur, 2000: The interaction between Hurricane Opal (1995) and a warm-core ring in the Gulf of Mexico. *Mon. Wea. Rev.*, in press.
- Kalnay, E., and Coauthors, 1996: The NCEP/NCAR 40-Year Reanalysis Project. *Bull. Amer. Meteor. Soc.*, **77**, 437–471.
- Khain, A., and I. Ginis, 1991: The mutual response of a moving tropical cyclone and the ocean. *Beitr. Phys. Atmos.*, **64**, 125–141.
- Koch, S. E., M. DesJardins, and P. J. Kocin, 1983: An interactive Barnes objective map analysis scheme for use with satellite and conventional data. *J. Climate Appl. Meteor.*, **22**, 1487–1503.
- Koteswaram, P., and C. A. George, 1957: The formation and structure of tropical cyclones in the Indian Sea area. *J. Meteor. Soc. Japan*, **35**, 309–322.
- Krishnamurti, T. N., W. Han, B. Jha, and H. S. Bedi, 1998: Numerical prediction of Hurricane Opal. *Mon. Wea. Rev.*, **126**, 1347–1363.
- Lawrence, M. B., B. M. Mayfield, L. A. Avila, R. J. Pasch, and E. N. Rappaport, 1998: Atlantic hurricane season of 1995. *Mon. Wea. Rev.*, **126**, 1124–1151.
- Lee, C. S., R. Edson, and W. M. Gray, 1989: Some large-scale characteristics associated with tropical cyclone development in the North Indian Ocean during FGGE. *Mon. Wea. Rev.*, **117**, 407–426.
- Marks, F. D., and L. K. Shay, 1998: Landfalling tropical cyclones: Forecast problems and associated research opportunities. *Bull. Amer. Meteor. Soc.*, **79**, 867–876.
- Merrill, R. T., 1988a: Characteristics of upper-tropospheric environmental flow around hurricanes. *J. Atmos. Sci.*, **45**, 1665–1677.
- , 1988b: Environmental influences on hurricane intensification. *J. Atmos. Sci.*, **45**, 1678–1687.
- , 1993: Tropical cyclone structure. *Global Guide to Tropical Cyclone Forecasting*, G. J. Holland, Ed., World Meteorological Organization, 2.1.1–2.60.
- , and C. S. Velden, 1996: A three-dimensional analysis of the outflow layer of Supertyphoon Flo (1990). *Mon. Wea. Rev.*, **124**, 47–63.
- Molinari, J., 1993: Environmental controls on eyewall cycles and intensity changes in Hurricane Allen (1980). *Tropical Cyclone Disasters*, J. Lighthill et al., Eds., Peking University Press, 328–337.
- , 1998: Hurricane–trough interactions: How do they work? Preprints, *Symp. on Tropical Cyclone Intensity Change*, Phoenix, AZ, Amer. Meteor. Soc., 169–170.
- , and D. Vollaro, 1989: External influences on hurricane intensity. Part I: Outflow layer eddy angular momentum fluxes. *J. Atmos. Sci.*, **46**, 1093–1105.
- , and —, 1990: External influences on hurricane intensity. Part II: Vertical structure and response of the hurricane vortex. *J. Atmos. Sci.*, **47**, 1902–1918.
- , S. Skubis, and D. Vollaro, 1995: External influences on hurricane intensity. Part III: Potential vorticity structure. *J. Atmos. Sci.*, **52**, 3593–3606.
- , —, —, F. Alsheimer, and H. E. Willoughby, 1998: Potential vorticity analysis of tropical cyclone intensification. *J. Atmos. Sci.*, **55**, 2632–2644.
- Montgomery, M. T., 1998: Vortex intensification by convectively forced vortex Rossby waves. Preprints, *Symp. on Tropical Cyclone Intensity Change*, Phoenix, AZ, Amer. Meteor. Soc., 21.
- , and B. Farrell, 1993: Tropical cyclone formation. *J. Atmos. Sci.*, **50**, 285–310.
- , and R. J. Kallenbach, 1997: A theory for vortex Rossby waves and its application to spiral bands and intensity changes in hurricanes. *Quart. J. Roy. Meteor. Soc.*, **123**, 435–465.
- , and J. Enagonio, 1998: Tropical cyclogenesis via convectively forced vortex Rossby waves in a three-dimensional quasigeostrophic model. *J. Atmos. Sci.*, **55**, 3176–3207.
- Neuman, C. J., 1997: National plan for tropical cyclone research. FCM Rep. FCM-P25-1991, 100 pp. [Available from Office of the Federal Coordinator for Meteorological Services and Supporting Research, 8455 Colesville Rd., Suite 1500, Silver Spring, MD 20910.]
- Palmer, C. E., 1951: On high-level cyclones south of the maximum westerlies. *Trans. Amer. Geophys. Union*, **32**, 683–696.
- Pfeffer, R. L., and M. Challa, 1981: A numerical study of the role of eddy fluxes of momentum in the development of Atlantic Hurricanes. *J. Atmos. Sci.*, **38**, 2393–2398.
- Poe, G., 1990: Optimum interpolation of imaging microwave radiometer data. *IEEE Trans. Geosci. Remote Sens.*, **28**, 800–810.
- Ramage, C. S., 1959: Hurricane development. *J. Meteor.*, **16**, 227–237.
- Riehl, H., 1948: On the formation of typhoons. *J. Meteor.*, **5**, 247–264.
- , 1950: A model of hurricane formation. *J. Appl. Phys.*, **21**, 917–925.
- Rotunno, R., and K. A. Emanuel, 1987: An air–sea interaction theory for tropical cyclones. Part II: Evolutionary study using a non-hydrostatic axisymmetric numerical model. *J. Atmos. Sci.*, **44**, 542–576.
- Sadler, J. C., 1976: A role of the tropical upper tropospheric trough in early season typhoon development. *Mon. Wea. Rev.*, **104**, 1266–1278.
- Schmetz, J., S. A. Tjemkes, M. Gube, and L. van de Berg, 1997: Monitoring deep convection and convective overshooting. *Meteor. Adv. Space Res.*, **19**, 433–441.
- Shapiro, L. J., and H. E. Willoughby, 1982: The response of balanced hurricanes to local sources of heat and momentum. *J. Atmos. Sci.*, **39**, 378–394.
- Shay, L. K., P. G. Black, A. J. Mariano, J. D. Hawkins, and R. L. Elsberry, 1992: Upper ocean response to hurricane Gilbert. *J. Geophys. Res.*, **97** (12), 20 227–20 248.
- , G. J. Goni, and P. G. Black, 2000: Effects of a warm oceanic feature on Hurricane Opal. *Mon. Wea. Rev.*, in press.
- Shi, J. J., S. Chang, and S. Raman, 1997: Interaction between Hurricane Florence (1988) and an upper-tropospheric westerly trough. *J. Atmos. Sci.*, **54**, 1231–1247.
- Simpson, R. H., 1952: Evolution of the kona storm, a subtropical cyclone. *J. Meteor.*, **9**, 24–35.
- , 1974: The hurricane disaster potential scale. *Weatherwise*, **27**, 169–186.
- Velden, C. S., 1987: Satellite observations of Hurricane Elena (1985) using the VAS 6.7 micron “water-vapor” channel. *Bull. Amer. Meteor. Soc.*, **68**, 210–215.
- , and T. Olander, 1998: Bispectral satellite technique for delineating intense convection: Applications to tropical cyclones. *Extended Abstracts, Ninth Conf. on Satellite Meteorology and Oceanography*, Paris, France, Amer. Meteor. Soc., 458–461.
- , W. S. Olson, and B. A. Roth, 1989: Tropical cyclone center-fixing using DMSP SSM/I data. Preprints, *18th Conf. on Hurricanes and Tropical Meteorology*, San Diego, CA, Amer. Meteor. Soc., J36–J39.
- , C. M. Hayden, S. J. Nieman, W. P. Menzel, S. Wanzong, and J. S. Goerss, 1997: Upper-tropospheric winds derived from geostationary satellite water vapor observations. *Bull. Amer. Meteor. Soc.*, **78**, 173–195.
- , T. L. Olander, and S. Wanzong, 1998: The impact of multi-spectral GOES-8 wind information on Atlantic tropical cyclone track forecasts in 1995. Part I: Dataset methodology, description and case analysis. *Mon. Wea. Rev.*, **126**, 1202–1218.
- Willoughby, H. E., 1990: Temporal changes of the primary circulation in tropical cyclones. *J. Atmos. Sci.*, **47**, 242–264.
- , and P. G. Black, 1996: Hurricane Andrew in Florida: Dynamics of a disaster. *Bull. Amer. Meteor. Soc.*, **77**, 543–549.
- , J. A. Clos, and M. G. Shoreibah, 1982: Concentric eyes, secondary wind maxima, and the evolution of the hurricane vortex. *J. Atmos. Sci.*, **39**, 395–411.

- Wu, C.-C., and K. A. Emanuel, 1993: Interaction of a baroclinic vortex with background shear: Application to hurricane movement. *J. Atmos. Sci.*, **50**, 62–76.
- , and —, 1994: On hurricane outflow structure. *J. Atmos. Sci.*, **51**, 1995–2003.
- Yanai, M., 1961: A detailed analysis of typhoon formation. *J. Meteor. Soc. Japan*, **39**, 282–309.
- Zehr, R. M., 1998: Vertical wind shear and tropical cyclone intensity. Preprints, *Symp. on Tropical Cyclone Intensity Change*, Phoenix, AZ, Amer. Meteor. Soc., 124–126.